

AN EXPERIMENT IN NUMERICAL PREDICTION IN EQUATORIAL LATITUDES

T. N. Krishnamurti*

Department of Meteorology and Oceanography
Naval Postgraduate School
Monterey, California 93940

Contract No: MIPR ES-7-967
Project No. 6698
Task No. 669802
Work Unit No. 66980201

NPS-51KJ8081A;

SR-4.

Scientific Report No. 4

October 1968

Contract Monitor: Thomas J. Keegan
Meteorology Laboratory

Distribution of this document is unlimited. It may be released
to the Clearing House, Department of Commerce,
for sale to the general public.

Prepared

for

AIR FORCE CAMBRIDGE RESEARCH LABORATORIES
OFFICE OF AEROSPACE RESEARCH
UNITED STATES AIR FORCE
BEDFORD, MASSACHUSETTS 01730

*Department of Meteorology
Florida State University
Tallahassee, Florida 32306

Qualified requestors may obtain additional copies from the Defense Documentation Center. All others should apply to the Clearinghouse for Federal Scientific and Technical Information.

AN EXPERIMENT IN NUMERICAL PREDICTION IN EQUATORIAL LATITUDES

T. N. Krishnamurti*

Department of Meteorology and Oceanography
Naval Postgraduate School
Monterey, California 93940

Contract No: MIPR ES-7-967
Project No. 6698
Task No. 669802
Work Unit No. 66980201

Scientific Report No. 4

October 1968

Contract Monitor: Thomas J. Keegan.
Meteorology Laboratory

Distribution of this document is unlimited. It may be released
to the Clearing House, Department of Commerce,
for sale to the general public.

Prepared
for

AIR FORCE CAMBRIDGE RESEARCH LABORATORIES
OFFICE OF AEROSPACE RESEARCH
UNITED STATES AIR FORCE
BEDFORD, MASSACHUSETTS 01730

*Department of Meteorology
Florida State University
Tallahassee, Florida 32306

NAVAL POSTGRADUATE SCHOOL
Monterey, California

Rear Admiral R. W. McNitt, USN
Superintendent

R. F. Rinehart
Academic Dean

This task was supported by: U. S. Air Force Cambridge Research Laboratories
Research Project MIPR-ES-7-967

ABSTRACT

In order to obtain the dynamical structure of the tropical atmosphere in equatorial latitudes a short range prediction experiment is proposed. The initial field contains the intertropical convergence zone and associated disturbances over western Pacific Ocean during March 1965. A complete initial state is constructed using a consistent balance system of equations. The procedure involves construction of pressure, temperature and vertical motion distributions starting from an observed rotational part of the wind field. It is shown that this procedure, whose validity assumes a small Rossby number, does not yield a realistic structure of the vertical motion. A short range prediction with a multi-level prediction model yields some interesting solutions in the vicinity of the intertropical convergence zone. During the first 18 hours of prediction an adjustment of the motion and the mass field ensues with gravity inertia oscillations. A detailed discussion of some dynamical aspects at 24 hours is presented. An important feature of the model is a parameterization of cumulus convection as a function of large-scale moisture convergence. The role of cumulus scale heating in the vicinity of the intertropical convergence zone is explored by carrying out experiments with and without diabatic heating.

List of symbols

a	fraction (or percent) of synoptic scale area covered by convective clouds
C_D	drag coefficient
C_p	specific heat of air at constant pressure
e	vapor pressure of air. Subscript w refers to water surface
E_v	evaporation from sea surface
f, f_0	Coriolis parameter, and a mean value of the Coriolis parameter (respectively)
F_x, F_y	friction force per unit mass of air
F_S	flux of sensible heat from ocean to the atmosphere
F_θ, F_q	Diffusion of heat and moisture, respectively
g	acceleration of gravity
H, M	heat and moisture sources and sinks, respectively
H_S, H_L	sensible and latent heat (respectively) per unit mass of air
h	terrain height above sea level
i, j, k	unit vectors along zonal, meridional and vertical directions
I	net moisture convergence in a unit vertical column extending from 900 millibars to the top of the atmosphere (100 mb)
ITCZ	intertropical convergence zone
K_E	eddy kinetic energy
K_Z	kinetic energy of mean zonal flow
ℓ	number of grid points along x-axis
L	latent heat of vaporization of air
m	map projection factor
p, p_0	pressure and a standard pressure (= 1000 mb), respectively
P_E	eddy potential energy

P_Z	potential energy of mean zonal flow
Q	any arbitrary variable
Q_1	amount of moisture required to replace an ambient moisture sounding by a local moist adiabat
Q_2	amount of moisture required for condensation warming to replace an ambient temperature sounding by a local moist adiabat
R	gas constant
q	specific humidity
Ro	Rossby number
T, θ	temperature and potential temperature of air, respectively
T_a	temperature of air at anemometer level, assumed same as T_{1000} in this study
T_S, q_S	temperature and specific humidity (respectively) of a parcel raised vertically above the 900 millibar surface with no lateral mixing
T_W	temperature of water
u, v, w	zonal, meridional and vertical (p) velocity
V, \mathbf{V}	total horizontal wind speed and wind vector, respectively
ω_C	average vertical velocity over region occupied by convective clouds inside a synoptic-scale elementary area
$\tilde{\omega}$	average vertical velocity over a region not occupied by convective clouds inside a synoptic-scale elementary area
$\overline{\omega}$	synoptic scale vertical velocity
η_{mn}	coefficient of a 9-point local surface
x, y, p, t	independent variables
Z	height of constant pressure surface

θ_e	equivalent potential temperature
μ, κ	horizontal and vertical eddy diffusion coefficients
τ_x, τ_y	surface frictional stresses along the x and y axes
Δp	vertical grid distance
ϕ	geopotential height of pressure surface
ϕ_B	zonal mean geopotential on a boundary wall
ϕ	latitude
(I, J)	a reference grid point on the mercator map
ρ	density of air
$()_{1000}$	the subscript 1000 refers to the value at the 1000 millibar surface
ψ, ζ	streamfunction and relative vorticity
V_ψ	non-divergent part of the wind
σ	static stability parameter, $= - \frac{RT}{p\theta} \frac{\partial \theta}{\partial p}$
ζ_a	absolute vorticity
β	the beta parameter, $= \frac{\partial f}{\partial y}$
Π	Exner pressure, $= \frac{RT}{p\theta}$
χ	divergent part of the wind field, a velocity potential
$(-)$	bar refers to a zonal average
$()'$	primes at a symbol refer to departures from a zonal average

1. Introduction.

In the middle latitudes the formation of an extratropical storm is generally regarded as a baroclinic instability problem. The primary energy source that leads to large kinetic energy of extratropical vortices is the available potential energy. Phillips (1956) discussed the energetics of this class of disturbances in his numerical general circulation experiment.

Lack of understanding of the types of instabilities in the tropics has, so far, prevented the use of well defined numerical experiments to simulate the development of disturbances that are frequently portrayed from observations on weather maps.

Some success in the understanding of the formation and maintenance of a tropical storm (or hurricane) has been achieved through the works of Ooyama (1963), Charney and Eliassen (1964), Kuo (1965) and several others. The primary reason for the success of this work has been due to a recognition of what is called a conditional instability of the unsaturated tropical air mass. Unlike the baroclinic instability problem where disturbance with horizontal wavelengths of the order of 1000 or more kilometers have a maximum growth rate, for the tropical conditional instability the maximum growth rate is found for horizontal wavelengths of 5 to 10 kilometers in scale (Kuo, 1961). This latter scale is now recognized as the cumulus scale. Most active tropical disturbances contain this cumulus scale in the form of organized bands of convection. There is a certain cooperation of the large and small scale the nature of which is a central problem in tropical meteorology. The entire belt of tropics is frequently conditionally unstable, namely

$$-\frac{\partial \theta_e}{\partial p} < 0$$

(θ_e is the equivalent potential temperature and p is pressure.) This is observed from an examination of atmospheric soundings below the 500 mb surface. However, convective scale as manifested by satellite and aircraft observations of clouds, is present only over portions of the tropics. Thus, there is evidently a suppression of the convective motion over large areas of the tropics. This might be controlled by the large scale atmospheric dynamics.

A mere examination of the streamline features on a weather map does not, in general, give indications of where one should expect convective motion to be present or absent. Several tropical meteorologists present large quantities of weather maps showing merely the field of wind direction. The atmosphere being considerably more complicated, not many questions can be thus either asked or answered.

Because of large data voids in the tropics the age of discovery of new phenomena is not yet over. As an example of this one may cite the discovery of the climatological mean troughs of the upper tropical troposphere over the Atlantic and Pacific Oceans. These were deduced from commercial aircraft reports of upper winds during recent observational studies by Dean (1956) and Sadler (1967). These papers do not deal with either the three-dimensional structure or the dynamics of these climatological features. There is thus no wide recognition of the importance of these studies. The data is sufficient to portray cyclonic or anticyclonic streamline features on a constant pressure surface, but it is generally insufficient for study of the dynamical structure. Several climatological features of this kind must exist over the remaining vast uncharted oceanic

regions of the tropics. Through use of satellite cloud photographs it might be possible to locate regions where such disturbances are present.

This paper presents some features of the tropical circulations for one day, March 1, 1965, as part of an investigation which is being continued over a longer period of time. The study deals with the dynamics of the intertropical convergence zone. The approach is to construct a consistent three-dimensional distribution of motion, mass, temperature and moisture fields through use of diagnostic and prognostic numerical models. The large-scale horizontal wind speed in the tropics is of the order of 10 meters/sec while vertical motion, $\bar{\omega}$, is of the order 1 cm/sec (Baumhefner, 1968). The latter may be expressed by a relation of the form

$$\bar{\omega} = a \omega_c + (1-a) \tilde{\omega} \quad (1)$$

where 'a' is fraction of the synoptic scale area covered by convective clouds, ω_c and $\tilde{\omega}$ are respectively vertical motions in the cloud and outside the cloud in a unit area. Theories of parameterization of the small scale convective motion as a function of a larger scale motions enable us to determine the parameter 'a' subject to a number of approximations. $\bar{\omega}$ can be estimated from solution of balance equations and ω -equation or through numerical integration of primitive equations.

No description of the three-dimensional structure of a weather disturbance can be complete without a distribution of the motion field in the three dimensions. Any investigation of energetics, development and instability relies heavily on the distribution of vertical motion.

For phenomenon of small Rossby number ($Ro < 1$), a measure of the vertical motion may be obtained from a solution of the quasi-geostrophic

ω -equation or a more general balance ω -equation (Krishnamurti, 1968a). In investigations of phenomenon of low latitudes (like the intertropical convergence zone) where $Ro \approx 1$, the validity of the quasi-geostrophic or balance ω -equation is questionable. Primitive equation forecast models contain no approximation (except the quasi-static approximation, if the vertical equation of motion is a hydrostatic balance) and hence a short range forecast (using a quasi-geostrophic or balanced initial state) might yield a reasonable solution of the three-dimensional motion field which would be valid for large Rossby number. Generally, such an unbalanced initial state is expected to produce gravity inertia oscillations. These are damped oscillations and there is an ensuing adjustment of the dependent variables into a large Rossby number disturbance. Some map features of the initial state are lost as both the wind and the pressure field undergo a degree of adjustment. The process of adjustment of wind and pressure in low latitudes in the presence of the smaller convective scale is a very complicated and important theoretical problem. Simple formulations of this problem by Rosenthal (1965) and Matsuno (1966a) are important contributions.

We shall show in this paper, that the numerical solution of the primitive equations (starting from solutions of a diagnostic balance model) undergoes an adjustment, the theoretical nature of which is not quite clear, but the process is certainly of interest. It should be noted that the adjustment and the damping of the gravity inertial oscillation is brought about by the diffusion of momentum and potential temperature. The diffusion coefficients are selected somewhat arbitrarily in these studies; the choice was made by trial and error. In our study after

a period of approximately 12 hours these oscillations become very small in amplitude. We are thus able to present a description of the three-dimensional distribution of mass, moisture and motion field for large Rossby number phenomena through short range numerical prediction of atmospheric variables. Two questions that come up in the light of these comments regarding the oscillations are:

i) How good is the initial data for a description of the large scale distribution of the dependent variables in regions near the equator or in the tropics?

ii) How much of the initial map features is lost during this process of adjustment?

We are concerned here with a study of the intertropical convergence zone. There is a considerable amount of data in the western Pacific Ocean to describe the large-scale flow both at the surface level and up to the 200 millibar surface. This is borne out by a number of descriptive studies in this region (Yanai, 1961). This data is supplemented by a number of aircraft reports (AIREPS) that enable a better analysis of the 700 and 250 millibar charts. The initial analysis at the lowest levels contains features like a convergence line (the ITCZ). At the upper level features like warm high pressure cells are found to the north and south of the low level convergence line. The anticyclonic outflow from these upper level high pressure cells (size 1000nds of kilometer scale) is an easterly wind maximum over the equatorial latitudes and lies directly above the surface level convergence asymptotes. The damped oscillation of the prediction does not destroy these large-scale features. Hence, a description of the predicted fields may be considered a description

of the large-scale dynamical structure of the ITC. This is the principal motivation for carrying out this investigation.

2. A primitive Equation Model

(a) Advective scheme and basic equations:

The main features of the advective scheme are essentially the same as those proposed by the author, Krishnamurti, 1962. Similar quasi-Lagrangian schemes have been proposed by Leith (1964) and Ökland (1965). Leith carried out long-term numerical integrations in a general circulations model while Ökland proposed its use in short-term integrations for a two-level model. No non-linear advective terms $(V \cdot \nabla Q)$ appear explicitly in this formulation and thus no obvious non-linear computational instabilities are present. In a recent review of various problems, generally encountered in numerical weather prediction, Elsasser (1968) points out that Ökland's Lagrangian advective scheme was one of the important factors in the successful prediction of cyclogenesis over short time periods of the order of two days.

The main outline of advective scheme will be discussed here. Consider the basic system of the primitive equations expressed in the form

$$\frac{Du}{Dt} = A = -\omega \frac{\partial u}{\partial p} + fv - mg \frac{\partial z}{\partial x} + F_x \quad (2)$$

$$\frac{Dv}{Dt} = B = -\omega \frac{\partial v}{\partial p} - fu - mg \frac{\partial z}{\partial y} + F_y \quad (3)$$

$$\frac{D\theta}{Dt} = C = -\omega \frac{\partial \theta}{\partial p} + \frac{H}{C_p} \left(\frac{p_0}{p} \right)^{R/C_p} + F_\theta \quad (4)$$

$$\frac{Dq}{Dt} = D = -\omega \frac{\partial q}{\partial p} + M + F_q \quad (5)$$

$$\frac{D}{Dt} (Z_{1000} - h) = E = \omega_{1000} \frac{R}{1000 g} \theta_{1000} \quad (6)$$

$$\frac{\partial \omega}{\partial p} = - \left(\frac{\partial u}{\partial x} + \frac{\partial v}{\partial y} \right) \quad (7)$$

$$\frac{\partial z}{\partial p} = - \frac{R}{gp} \theta \left(\frac{p}{p_0} \right)^{R/C_p} \quad (8)$$

This may be regarded as a closed system for the seven variables u , v , θ , q , Z_{1000} , ω and $\frac{\partial z}{\partial p}$ or alternatively a closed system for u , v , θ , q , z and ω , with appropriate boundary conditions. $\frac{D}{Dt}$ is a quasi-Lagrangian operator given by

$$\frac{D}{Dt} \equiv \frac{\partial}{\partial t} + m \left\{ u \frac{\partial}{\partial x} + v \frac{\partial}{\partial y} \right\} \quad (9)$$

Here m is a map factor, in our case for a mercator projection expressed by the relation

$$m = \sin 85 \operatorname{cosec} (90 - \phi) \quad (10)$$

where ϕ is the latitude, $m = 1$ at $\phi = 15^\circ N$ and $15^\circ S$, at the equator

$m = 0.996$.

Equations (2) and (3) are the momentum equations,

(4) is a form of the thermodynamic energy equation. Equation (5) is a

statement for conservations of water vapor. Equation (6) is a tendency

equation of the pressure frame where the role of orography, h , is in-

cluded. (7) and (8) are, respectively, the continuity and hydrostatic

equations. Heat sources and sinks, H , and the moisture sources and

sinks, M , are discussed later in the paper. F_x and F_y , F_θ , and F_q repre-

sent frictional and diffusive transfers of momentum, heat and moisture,

and are also discussed later.

The principle of the quasi-Lagrangian advective scheme is to locate the past position (P) of a parcel on a pressure surface during each time step, the parcel arrives at a grid point Q (I, J) at the end of each time step, see figure 1. During the course of movement from P to Q non-conservative changes take place which are incorporated in the advected properties.

The iterative procedure utilizes a local surface over 9 points of figure 1 defined by the relation

$$Q_{xy} = \sum_{m=0}^2 \sum_{n=0}^2 \eta_{mn} X^m Y^n \quad (11)$$

The nine coefficients η_{mn} are predetermined for each point and do not vary during the course of the integration. X and Y are distances in the zonal and meridional directions between the central point I, J and the other 8 points of figure 1.

$$\text{Distance (PQ)} = \sqrt{X^2 + Y^2}.$$

Point P is determined by a predictor corrector successive approximation procedure, the first guess is defined by the relations

$$\left. \begin{aligned} X &= -u(Q)_{t-\Delta t} \Delta t \\ Y &= -v(Q)_{t-\Delta t} \Delta t \end{aligned} \right\} \quad (12)$$

The variables u, v, ω , z, θ , q, A, B, C, D and E are determined at the point P using relation (11) and the values of X and Y defined in equation (12).

Note that Δt is a time step; the subscript $t-\Delta t$ is the previous time period and t would be the current time for which a prediction is

desired. The first guess prediction of the dependent variables is carried out according to the relations,

$$\left. \begin{aligned}
 u(Q)_t &= u(P)_{t-\Delta t} + A(P)_{t-\Delta t} \Delta t \\
 v(Q)_t &= v(P)_{t-\Delta t} + B(P)_{t-\Delta t} \Delta t \\
 \theta(Q)_t &= \theta(P)_{t-\Delta t} + C(P)_{t-\Delta t} \Delta t \\
 q(Q)_t &= q(P)_{t-\Delta t} + D(P)_{t-\Delta t} \Delta t \\
 Z_{1000}(Q)_t &= Z_{1000}(P)_{t-\Delta t} + E(P)_{t-\Delta t} \Delta t
 \end{aligned} \right\} \quad (13)$$

$Z(Q)_t$ and $\omega(Q)_t$ are determined from the diagnostic relations (7) and (8).

The second guess defines a location of the point P through the relations

$$\left. \begin{aligned}
 X &= - \{u(P)_{t-\Delta t} + u(Q)_t\} \Delta t/2 \\
 Y &= - \{v(P)_{t-\Delta t} + v(Q)_t\} \Delta t/2
 \end{aligned} \right\} \quad (14)$$

Variables u , v , ω , Z , θ , and q are interpolated at point P (time $t-\Delta t$) and the prediction at point Q is carried out using the relations

$$\left. \begin{aligned}
 u(Q)_t &= u(P)_{t-\Delta t} + A(Q)_t \Delta t \\
 v(Q)_t &= v(P)_{t-\Delta t} + B(Q)_t \Delta t \\
 \theta(Q)_t &= \theta(P)_{t-\Delta t} + C(Q)_t \Delta t \\
 q(Q)_t &= q(P)_{t-\Delta t} + D(Q)_t \Delta t \\
 Z_{1000}(Q)_t &= Z_{1000}(P)_{t-\Delta t} + E(Q)_t \Delta t
 \end{aligned} \right\} \quad (15)$$

$Z(Q)_t$ and $\omega(Q)_t$ are again determined from equations (7) and (8).

This two-step predictor corrector is similar to Matsuno's (1966b) time differencing scheme for Eulerian and spectral equations (see also Lilly (1965)). Terms containing vertical advection, pressure gradients, Coriolis force, friction, heating and other non-conservative features on the right hand side of equations (2) through (7) are incorporated in A, B, C, D and E. A time step $\Delta t = 10$ minutes is used in the present study.

b) Domain of integration, distribution of variables:

The domain of integration extends from 104°E longitude to 128°W longitude over the Pacific. Northern and southern limits of the domain extend from 28°N to 28°S . The region between 152°W to 128°W is used to prescribe a cyclic continuity in the east-west direction. This is carried out by a quadratic interpolation of the initial analyzed data such that,

$$Q(104^\circ\text{E}) = Q(128^\circ\text{W}) \quad (16)$$

where Q is any analyzed variable. It must be noted that the initial state over the entire domain is a consistent balanced hydrostatic set, cyclic continuity merely removes east-west boundaries in both the diagnostic and prognostic studies presented here.

In a recent comparative study of several finite difference analogs for primitive equations, Grummeltvedt (1968) states that if integrations are performed for more than three days then more than 15 grid points per wavelength are needed to describe with accuracy the movement and development of the shortest wave which initially is carrying a significant part of the energy. This is an important result for numerical weather prediction. This would imply that for studies of development and

movement of a disturbance in the tropics, whose wavelength is of the order of 1000 km, a mesh size of the order of 60 km would be required. A fine mesh model will be widely used, when faster computers with larger core storage become available. Phase speed errors, through reduction of truncation errors, can be reduced appreciably by this procedure. In the present study we use a mesh size of 2° latitude by 2° longitude and its limitations are thus obvious. In certain large-scale general circulation models, mesh sizes of the order of 5° latitude are being used.

In the present study there is no staggering of variables in the horizontal; however, there is a staggering of dependent variables in the vertical. It is a five-level model and staggering permits all nine levels to be used. This vertical structure is primarily dictated by the nature of the dynamical and thermodynamic equations, see figure 2.

c) Boundary conditions for the primitive equation model

As mentioned earlier, there are no boundaries in the zonal direction in this study. Our basic grid extends from 28°N to 28°S . There is, however, an implicit north and south pole in the model. At the north and south poles we assume at each time step

$$\begin{aligned}
 Z_{1000} \text{ (North pole)} &= \sum_x Z_{1000} (28^\circ\text{N})/\ell \\
 \theta \text{ (North pole)} &= \sum_x \theta (28^\circ\text{N})/\ell \\
 q \text{ (North pole)} &= \sum_x q (28^\circ\text{N})/\ell \\
 Z_{1000} \text{ (South pole)} &= \sum_x Z_{1000} (28^\circ\text{S})/\ell \\
 \theta \text{ (South pole)} &= \sum_x \theta (28^\circ\text{S})/\ell \\
 q \text{ (South pole)} &= \sum_x q (28^\circ\text{S})/\ell
 \end{aligned}
 \tag{17}$$

u, v and w at the two poles are assumed zero during the integration. A linear interpolation between pole and 28° is used to calculate the values at 30°N and 30°S during each time step. These values were used as boundary conditions during the course of the integration. This scheme was found to be stable and values of the vertical motions, the most sensitive parameter of this model, do not become unreasonable. This boundary condition does not in any way represent the behavior of the real atmosphere at 30°N and 30°S.

d) The development in the primitive equation model

In quasi-geostrophic models development is generally discussed in terms of processes producing individual changes of vorticity via the vorticity equation. These changes are primarily attributable to the presence of fields of divergence and convergence. In primitive equation models surface development may be described via the following equations.

$$\omega_{1000} = - \int_{100}^{1000} \left(\frac{\partial u}{\partial x} + \frac{\partial v}{\partial y} \right) dp \quad (18)$$

$$\frac{D}{Dt} (Z_{1000} - h) = \omega_{1000} \frac{R}{p_0} \theta_{1000} \quad (18b)$$

If $h = 0$ (no terrain) and if the vertically integrated divergence is zero, then

$$\omega_{1000} = 0 \quad (19)$$

and

$$\frac{DZ_{1000}}{Dt} = 0 \quad (20)$$

i.e., parcels moving on the 1000-millibar surface will conserve their heights and no deepening or filling of surface systems is possible.

Up and downslope motions over large-scale terrain features permit development of surface systems such as upslope anticyclogenesis and a lee cyclogenesis. Net convergence leads to a sinking motion ($\omega_{1000} > 0$ and $\frac{DZ_{1000}}{Dt} > 0$), while the converse is true of net divergence. One would think that since the vertically integrated divergence is a small difference between large numbers (at each level) the results of such vertical integration will be very sensitive and only spurious results can be obtained. This, however, definitely is not the case. A balanced initial state starts out with minor gravity inertia oscillations which damp rapidly with time and very small and reasonable magnitudes of ω_{1000} are indeed produced by the time integrations, see figure 12. This has been verified by nearly all of the research workers who have integrated the primitive equations. A synoptic meteorologist finds it very difficult to understand this feature of the primitive equation models when he knows that he has only a limited success in the use of the so-called tendency equation. The apparent reason for this lies in the fact that a primitive equation model generates a dynamically consistent momentum field with sufficient accuracy such that the net divergence and tendencies are small, as is the case for the real atmosphere. Direct observations do not yield small net divergences or tendencies because winds usually are in error. A detailed, dynamic explanation of this process of adjustment would be of considerable synoptic interest.

In the vicinity of mountains ω_{1000} acquires magnitudes very close to that given by the lower boundary conditions of the ω -equation, i.e. $\omega_{1000} = -g\rho_{1000} W_{1000} \cdot \nabla h$. This, again, is somewhat surprising because in the primitive equation model, terrain h modifies ω_{1000} via a rather

complicated cycle of operations.

h modifies Z_{1000} via equation (6)

Z_{1000} determines Z via equation (8)

Z determines u, v via equations (2) and (3)

u, v determines ω_{1000} via equation (7)

The reason for this must again be that a dynamically consistent primitive balance is indeed obtained when the initial state is given by the balance equations. The nature of such a primitive balance in the vicinity of the equator, where the Rossby number is greater than unity, has not been explored in theory as yet.

3. Initialization

A primitive equation model is currently being used in operational weather prediction at the National Meteorological Center in the United States (Shuman and Hovermale, 1968). The initial wind field is obtained from a solution of the so-called linear balance equation. This relationship between the wind field and the pressure field does not permit any divergence or vertical motions at the initial time. A similar initial state was proposed for the Bushby and Timpson's (1967) model by Benwell and Bretherton (1967) in a recent paper. It is pointed out by the latter authors that this procedure suppresses inertio-gravitational oscillations. These ideas are by no means new, Charney (1955), Hinklemann (1951) and Smagorinsky et al (1965) have proposed the use of non-divergent initial states for integration of primitive equations. Phillips (1960), on the other hand, showed that an initial divergence equal to that prescribed by quasi-geostrophic dynamics would be required to suppress the unwanted gravity inertio-oscillations.

In this paper we propose a rather detailed diagnostic balance model to define a consistent initial state. Thus, initially both divergence and vertical motions are present. A part of our interest will be to describe the three-dimensional synoptic structure and the dynamics of the motion, mass, thermal and moisture variables at the initial state from balance equations. This study departs somewhat from earlier study on initialization by the author (Krishnamurti, 1968a); here we propose an initialization of the dependent variables across the equator in a tropical belt. This poses some problems if the streamfunction were to be obtained from observed geopotential heights, but it is a relatively simple matter if the streamfunction is deduced from the observed wind field. The initialization procedure is as follows:

(a) Streamfunction ψ

The nondivergent part of the wind \mathbb{V}_ψ is obtained from a solution of the equations

$$\nabla^2 \psi = \zeta \quad (21)$$

and

$$\mathbb{V}_\psi = |\mathbf{k} \times \nabla \psi \quad (22)$$

where ζ is the relative vorticity of the observed wind. Boundary conditions for ψ are obtained by the procedure outlined by Hawkins and Rosenthal (1965) (version 2 of their work). This particular choice of boundary condition permits no net mass flux from the domain; however, ψ is permitted to vary along the boundaries.

(b) Initial distribution of geopotential heights

The distribution of geopotential, $\phi = gZ$, is obtained by solving the balance equation

$$\nabla^2 \phi = \nabla \cdot f \nabla \psi + 2J \left(\frac{\partial \psi}{\partial x}, \frac{\partial \psi}{\partial y} \right) \quad (23)$$

Since $\psi(x, y, p)$ is known the right hand side is defined in the domain and the solution of this elliptic equation is a straightforward problem.

At the boundaries we assume ϕ to be given by the relation

$$\phi_B = \bar{\phi} + f_0 (\psi - \bar{\psi}) \quad (23a)$$

ϕ_B is the value of ϕ at the northern or southern walls at 28°N or 28°S .

$\bar{\phi}$ is the zonal mean value of ϕ obtained from observations of geopotential height of the northern or southern wall.

$$f_0 = 10^{-4} \text{ sec}^{-1} \text{ at northern wall,}$$

$$\text{and } f_0 = -10^{-4} \text{ sec}^{-1} \text{ at southern wall.}$$

ψ is the value of the streamfunction at any point along the wall and

$\bar{\psi}$ the zonal mean value along that wall.

The initial distribution of potential temperature is given by

$$\theta = -\frac{p}{R} \left(\frac{p_0}{p} \right)^{R/C_p} \frac{\partial \phi}{\partial p} \quad (24)$$

Potential temperatures computed by this procedure were found to depart by as much as 3 degrees in the middle latitudes from observations.

Maximum departures were of the order of 5 degrees at lower levels.

This difficulty could have been overcome by using observed temperatures directly in the model; this, however, would cause the sacrifice

of the initial balance relationship of the variables. It is not

a priori clear how serious an effect this would have had on the initial amplitudes of gravity inertio-oscillations.

(c) Divergent part of the wind, χ , and vertical velocity

A detailed analysis of the system of equations required to solve for χ and ω is presented elsewhere by the author (Krishnamurti, 1968a).

Here we shall merely present the equations and their boundary conditions.

Omega equation

$$\begin{aligned}
 \nabla^2 \sigma \omega + f^2 \frac{\partial^2 \omega}{\partial p^2} &= f \frac{\partial}{\partial p} J(\psi, \zeta_a) + \pi \nabla^2 J(\psi, \theta) + f \frac{\partial}{\partial p} g \frac{\partial}{\partial p} \left[\frac{\partial \tau_y}{\partial x} - \frac{\partial \tau_x}{\partial y} \right] \\
 &- 2 \frac{\partial}{\partial t} \frac{\partial}{\partial p} J\left(\frac{\partial \psi}{\partial x}, \frac{\partial \psi}{\partial y}\right) - f \frac{\partial}{\partial p} (\zeta \nabla^2 \chi) \\
 &- \frac{R}{C_p} \nabla^2 H + f \frac{\partial}{\partial p} \left(\omega \frac{\partial}{\partial p} \nabla^2 \psi \right) \\
 &+ f \frac{\partial}{\partial p} (\nabla \omega \cdot \nabla \frac{\partial \psi}{\partial p}) - f \frac{\partial}{\partial p} \{ \nabla \chi \cdot \nabla \zeta_a \} \\
 &- \pi \nabla^2 \{ \nabla \chi \cdot \nabla \theta \} - g \frac{\partial}{\partial p} \frac{\partial}{\partial y} \frac{\partial \psi}{\partial t}
 \end{aligned} \tag{25}$$

Continuity equation

$$\nabla^2 \chi = \frac{\partial \omega}{\partial p} \tag{26}$$

Vorticity equation

$$\begin{aligned}
 \nabla^2 \frac{\partial \psi}{\partial t} &= - J(\psi, \zeta_a) + \nabla \chi \cdot \nabla \zeta_a + \zeta_a \nabla^2 \chi \\
 &- \omega \frac{\partial}{\partial p} \nabla^2 \psi - \nabla \omega \cdot \nabla \frac{\partial \psi}{\partial p} - g \frac{\partial}{\partial p} \left[\frac{\partial F_y}{\partial x} - \frac{\partial F_x}{\partial y} \right]
 \end{aligned} \tag{27}$$

Boundary conditions

$$\text{At } p = 100 \text{ mb, } \omega = 0$$

$$\text{At southern wall, } y = y_1, \omega = \chi = \frac{\partial \psi}{\partial t} = 0$$

$$\text{At northern wall, } y = y_2, \omega = \chi = \frac{\partial \psi}{\partial t} = 0$$

$$\text{At } p = 1000 \text{ mb, } \omega = -g \frac{1000}{R \theta_{1000}} \left[J(\psi, h) - \nabla \chi \cdot \nabla h \right]$$

The solutions for ω , χ and $\frac{\partial \psi}{\partial t}$ are obtained by a successive approximation procedure. This involves three-dimensional relaxation for ω and two-dimensional relaxation for χ and $\frac{\partial \psi}{\partial t}$. These three equations are coupled. Conditions for ellipticity of these equations are discussed by Krishnamurti (1968a).

F_x and F_y are frictional forces per unit mass of air, along the x and y axis; H is net diabatic heating per unit mass of air. These are discussed in some detail in a separate section of this paper. The same forms of friction and heating are retained in the initialization and prediction equations.

The total initial wind is given by

$$\mathbf{V} = \left(-\frac{\partial \psi}{\partial y} - \frac{\partial \chi}{\partial x} \right) \mathbf{i} + \left(\frac{\partial \psi}{\partial x} - \frac{\partial \chi}{\partial y} \right) \mathbf{j} \quad (28)$$

Initial distribution of moisture is a scalar hand analysis of relative humidity at standard meteorological levels, this is converted into fields of specific humidity q at the 900, 700, 500 and 300 millibars surfaces. The closed system of initial dependent variables are u , v , ω , Z , θ and q , figure 2 shows the vertical staggering of variables.

4. Diabatic heating and parameterization of cumulus scale

In the present model diabatic heating per unit mass of air is split into two components.

$$H = H_S + H_L \quad (29)$$

where H_S is the transfer of sensible heat from the ocean;

H_L is the release of latent heat.

We have not considered radiative effects.

(a) Sensible heat flux:

A simple flux formula (Jacobs, 1951), was used to define this quantity.

$$F_S = 0.0329 V (T_w - T_a) \quad (30)$$

The unit of flux, F_S , is mb meter sec⁻¹, V being the wind speed in meters/sec at anemometer level and $(T_w - T_a)$ the temperature difference between water at the ocean's surface and air at the anemometer level. The constant of proportionality has dimensions mb/°C. The rate of heating H_S may be expressed by the relation

$$H_S = g \frac{\partial F_S}{\partial p} \quad (31)$$

Potential temperature θ is a dependent variable and it appears at the 900, 700, 500 and 300 millibar surfaces. It is assumed that sensible heat transfer modifies the potential temperature of the air at the 900 millibar surface, and the flux, F_S , is assumed zero at 800 mb and above.

We express sensible heat at 900 millibar surface by the formula

$$\begin{aligned} H_S &= \frac{9.81}{100} 0.0329 V (T_w - T_a) \\ &= 0.00323 V (T_w - T_a) \end{aligned} \quad (32)$$

Here H_S has units meter² sec⁻³. If the air-sea temperature difference is of the order of 1°C and the wind speed is of the order 10 mps, then a change of one degree in potential temperature may be expected over a 24-hour period. This would require a representative analysis of the initial distribution of $(T_w - T_a)$ over the oceans. Because of general

lack of data only a rather smooth representation of this field is possible at this time. Radiative cooling is a serious omission of the present study because it is also of the order of a degree centigrade per day.

(b) Latent heat

H_L may again be divided into two forms of latent heat, stable and conditionally unstable. The former may be important in regions of dynamic ascent of moist and absolutely stable air. The latter may be important if there are regions where certain prescribed conditions for the evolution of cumulus scale convective elements are met. For the present we have omitted the stable form of latent heat as the tropical air mass is generally known to be conditionally unstable in the lower troposphere and our interest in this study is an equatorial, tropical belt.

The procedure for parameterization of the cumulus scale as a function of the large-scale motion with the mutual modification of the two scales is carried out along the lines of Kuo's (1965) formulation for a tropical storm.

Heat is released if the following criteria are met:

i) $-\frac{\partial \theta_e}{\partial p} < 0$ at any level above 1000 millibars. This measures the moist conditional instability.

ii) Net moisture convergence, $I > 0$, in vertical columns. The column extends from the top of the friction layer to the top of atmosphere (100 mb).

The heating function, H_L , is defined by the relation:

$$H_L = C_p \frac{g}{\Delta t} (T_S - T) \quad (33)$$

Where $(T_S - T)$ is the temperature difference between cloud element and tropical environment; C_p is the specific heat of air at constant pressure; Δt is a cloud time scale, where in a time integration problem we use Δt = the time step of the primitive equation model (Kuo, 1965); and "a" is a measure of the fraction of the grid scale area covered by active convective elements.

The calculation of "a" involves determining the following three integrals.

Net moisture convergence above friction layer.

$$I = \frac{1}{g} \int_{900}^{p_T} v \cdot q \, v \, dp - \frac{\omega_{900} q_{900}}{g} \quad (34)$$

$$Q_1 = \frac{1}{g\Delta t} \int_{900}^{p_T} (q_S - q) \, dp \quad (35)$$

$$Q_2 = \frac{1}{g\Delta t} \int_{900}^{p_T} \frac{C_p}{L} (T_S - T) \, dp \quad (36)$$

$$\text{and} \quad a = I / (Q_1 + Q_2) \quad (37)$$

T_S and q_S are respectively the temperature and specific humidity of a parcel raised dry adiabatically from 900 millibar surface to the lifting condensation level and then moist adiabatically to a level p_T where T_S intersects the environmental temperature. A detailed analysis of this parameterization procedure and aspects of calculation are discussed elsewhere by the author (Krishnamurti, 1968b). In this earlier study diagnostic calculations of vertical motions and various friction layer parameters were evaluated. It was shown that convective banded motions as revealed by airborne radar and that calculation of vertically

integrated moisture convergence and the field of the parameter "a" exhibit reasonable correlations. In the initialization and prediction phase of the present study the heating function is evaluated according to the flow chart, figure 3, which is self explanatory.

Large scale dynamical prediction of tropical disturbances including a formal parameterization of the cumulus convection have been carried out by Manabe and Smagorinsky (1967). It would be pertinent to review their parameterization procedure. In their general circulation model moist convective heating and condensation takes place when the lapse rate tends to become super-moist adiabatic and relative humidity tends to exceed 100 per cent. During this situation a convective adjustment is forced upon the numerical solution in such a way as to make the relative humidity and the equivalent potential temperature uniform in the unstable layer. Furthermore this adjustment is carried out in such a way as to keep the sum of potential, internal, and latent energy invariant. One of the obvious limitations of this procedure is that no convective process on small scale is permitted if relative humidity < 100 per cent. Synoptic experience in the tropics is quite to the contrary (e.g. Riehl, 1945; Baumhefner, 1968). Manabe and Smagorinsky (1967) discuss a rather interesting tropical disturbance that forms in their long-term general circulation experiment. Its large-scale structure is quite similar to that of a weak tropical storm, although a large inner core of this disturbance is very moist. The parameterization procedure that has been adopted here permits convective heat and moisture flux in the vertical direction even when the relative humidity is less than 100 per cent. However, this scheme presently suffers from the lack of a

built in check on convective adjustment which would control vertical soundings and force them to look like their atmospheric counterparts. Such a built-in convective adjustment is considered essential for long-term general circulations experiments. In this experiment calculations were extended by time steps to 48 hours and no severe problems such as supersaturations or super-moist adiabatic instabilities were found.

Kuo's scheme, used in this study, behaves roughly in the following manner:

A conditionally unstable region initially experiencing a net convergence of moisture flux, $I > 0$, is modified in a matter of a few hours so that large-scale values of T approach T_S , and q approaches q_S . This causes "a" to become smaller and the region to become sufficiently moist that further mass flux into the region begins to bring in relatively drier air and I changes sign to $I < 0$. When this happens we cease to parameterize the convective scale.

(c) Evaporation and precipitation

Conservation of water vapor is given by equation (5). Where M represents the net sources and sinks of water per unit mass of air.

Rohwer (1931) expresses evaporation from the ocean surface, E_v , by the relation:

$$E_v = (2.6 + 7.7 V_{1000}) (0.98 e_\omega - e_{1000}) / (24 \times 3600). \quad (38)$$

The units of E_v are $\text{gm}/(\text{cm}^2 \text{ sec})$; V_{1000} is the 1000 millibar wind in meters/sec; e_ω is the saturation vapor pressure in millibars at the temperature of the water's surface; and e_{1000} is the vapor pressure of air at the 1000 millibar surface. No attempt was made to vary the roughness constant for variable wind speeds over the oceans. Over land areas

E_v was set equal to zero.

Webb (1960) has critically reviewed the use of such an empirical formula for estimating evaporation and states that studies over Lake Eucumbe show that error would be within 10 per cent.

Precipitation was assumed to be entirely convective and was evaluated at each layer using Kuo's parameterization procedure, figure 3.

$$P_K = \frac{C_p a (T_S - T)}{L \Delta t} \quad (39)$$

K refers to the vertical level and P_K has the units sec^{-1} .

In our calculations the atmosphere is divided into four layers, 1000-800, 800-600, 600-400 and 400 to 200 millibars. Evaporation is only permitted in the lowest layer, and M is accordingly defined by the relation:

$$M = g \frac{E_v}{\Delta p} - \frac{C_p a (T_S - T)}{L \Delta t} \quad (40)$$

with $M = - \frac{C_p a (T_S - T)}{L \Delta t}$ in the other three layers. Δp is the thickness of the lowest layer.

5. Surface friction and diffusion terms of model

These terms, F_x and F_y , in the momentum equations contain two parts in this model:

- i) Subgrid scale lateral and vertical diffusion of momentum and
- ii) effect of surface wind stress.

This formulation is almost similar to that used by Mintz (1964) in his general circulation studies.

We write:

$$F_x = \mu m^2 \nabla^2 u + \kappa \frac{\partial^2 u}{\partial p^2} + g \frac{\partial \tau_x}{\partial p} \quad (41)$$

and

$$F_y = \mu m^2 \nabla^2 v + \kappa \frac{\partial^2 v}{\partial p^2} + g \frac{\partial \tau_y}{\partial p} \quad (42)$$

μ is a lateral eddy diffusion coefficient whose value in the present experiment is $5 \times 10^4 \text{ meter}^2 \text{ sec}^{-1}$ and κ is a vertical eddy diffusion coefficient whose value in the present experiment is $2 \times 10^{-2} \text{ mb}^2 \text{ sec}^{-1}$. The primary role of sub-grid scale lateral and vertical diffusion of momentum is to remove energy from the smallest permitted scales. It cannot represent physical subgrid scale processes in the horizontal or vertical, such as mesoscale horizontal jets or cumulus convection. It is found that absence of vertical diffusion κ gives rise to rather large horizontal wind speeds at the lowest levels within a 48-hour forecast period. Calculations did not appear to be critically dependent on the choice of the lateral coefficient.

Surface frictional stresses τ_x and τ_y are defined in terms of a surface roughness constant applied at the lower level, $p = 1000 \text{ mb}$.

$$\tau_x = C_D \rho \sqrt{u^2 + v^2} u \quad (43)$$

$$\tau_y = C_D \rho \sqrt{u^2 + v^2} v \quad (44)$$

C_D is the drag coefficient, whose value in the present experiment is 2.5×10^{-3} .

Surface stresses prescribed in this manner provide a crude boundary layer for our model between the 1000 and 900 millibar surfaces. Vertical motions at the 900 millibars are influenced significantly by

the presence of this effect. Frictional convergence of mass enhances low-level convergence of moisture and the latter prescribes a percent area of convective cloud distribution in our model. A discussion of these aspects is presented with the results of the numerical experiment.

6. A description of the Initial State: March 1, 1965, 1200 Z.

It is not possible to describe all of the scalar fields that define the initial state. A selection of some of the pertinent fields is presented here.

a) Streamlines of the observed wind field at 1000 and 200 millibar surfaces. Figures 4a and 4b, respectively, portray the streamlines (solid lines) and isotachs (dashed lines) at these two levels.

The following synoptic features of the intertropical convergence zone may be noted at the lower level. An asymptote of convergence extends from 152°W to about 144°E near 5° north latitude. The speed field along this asymptote is quite variable. Wind speed ranges from 5 to 25 knots over most of the map. There appears to be no simple structure for the isotach field in the vicinity of this asymptote of convergence. Wind speed maxima can be found along and north of this asymptote.

There is a belt of easterlies over most of the northern hemispheric portion of the analysis. An asymptote of convergence near 108°E is shown as a part of a cyclonic eddy at 3°N near 140°E. In the southern hemispheric tropics interesting features are the two cyclonic disturbances at 17°S, 110°E and at 15°S, 129°E. The speed field is shown to be somewhat organized in these disturbances. Over the rest of the Southern Hemisphere there are no well marked centers.

At 200 mb there are two regions of westerly wind maxima, one in the northwestern portion of the map over eastern Asia, and another over central Australia in the Southern Hemisphere. Over the equatorial latitudes a broad easterly current with speeds near 40 knots prevails. Four anticyclonic circulation centers (two in each hemisphere) constitute an important part of the upper-level flow. There are several other transient centers that are portrayed in the streamline analysis of this chart.

b) Moisture analysis at 900 millibar surface: Moisture analysis was carried out by first using all available stations at the surface level. A satellite nephanalysis (valid at approximately this time) was used as an underlay and the surface streamline features were used to complete the subjective distribution of relative humidity at 1000, 850, 700 and 500 millibar surfaces. The upper levels (850, 700 and 500) were arrived at by subjective examination of cloud cover, upper level data and the surface analysis. The relative humidity does not exceed saturation values on the large scale at any point. The analysis is very subjective and the available information is merely a guide. The distribution of the moisture variable is very poorly defined, hence it is somewhat unrepresentative. The initial values of specific humidity at 900 (interpolated between 1000, 850 millibars) are shown in figure 5(a). A moisture maximum is found north of Australia in the equatorial Pacific Ocean. It has values of specific humidity $> 18 \text{ gm/kgm}$. Another moisture maxima center with values close to 20 gm/kgm lies northeast of Australia and just south of the equator. Over the continent of Australia air is fairly dry, values being close to 5 gm/kgm . Over most of the equatorial

tropics values are near 15 gm/kgm. There is a gradual decrease of moisture between 16°N and 28°N to around 6 gm/kgm near 28°N.

Because of the uncertainty in the analysis of the moisture variable a prediction experiment was also carried out with uniform initial relative humidity at each pressure surface. This experiment is discussed separately below.

c) Temperature distribution in the middle troposphere: 500 millibar temperatures are shown in figure 5(b). Thermal structure over the central Pacific is characterized by two nearly isothermal warm centers with temperature around 269°K. These warm regions define the warm core structure of the anticyclones that extends to the 200 millibar surface; see figure 4(b).

In the northern and southern portions of the maps two well-marked baroclinic zones are present. They define regions where wind maxima are found at the 200 millibar surface, figure 4(b). The active portion of the intertropical convergence zone lies in the vicinity of 3°N and 140°E. In the middle troposphere mesoscale temperature anomalies are likely to be present over this region. The smooth large-scale isothermal patterns could be interpreted either as a lack of smaller scale data or an efficient lateral and vertical mixing process. This could be possible if vertical momentum exchange in the convective region reduces the vertical wind shear (Gray, 1967).

Sea surface temperatures were obtained from the monthly mean charts produced by U.S. Bureau of Commercial Fisheries (1962) and Moyskoi Atlas (1953) and were kept fixed during the experiment. Terrain height distributions were obtained from the tabulations of Berkofsky and Bertoni (1960).

d) Satellite cloud cover: During this period (March 1-3, 1965) TIROS X made a few passes and relevant pictures of cloud cover. Figure 6 (a and b) shows the cloud cover from approximately 130°E to 180°E and between 20°N and 20°S . The intertropical convergence zone is very well marked with bright clouds near 4° North between 160°E and 180°E on March 1. It is somewhat more extended and brighter on the 2nd and again well marked at about the same latitude on the 3rd. In the vicinity of 170°E and 15°S a well-marked cloud band oriented northwest-southeast is observable on all three days. On the 1st and 2nd a bright band of cloud cover is also persistent in the region 130°E to 140°E and 10°S to 20°S . This is over north central and north western Australia. The three above-mentioned regions of intense cloud cover are found in the vicinity of cyclonic surface systems and asymptotes of low-level convergence, figure 4(a). Over other regions the amount of cloudiness is variable during the three-day period. The picture time in each case is within 6 hours of the synoptic time of analysis.

No attempt will be made to relate each cloud feature observed on these TIROS passes with results of computations. Such an attempt would be futile at the present state of our work. Some reference will be made to the observed cloud cover, at least in its larger-scale context, in the following sections.

We shall next present some of the results of the initialization from the balance equations.

e) Initial streamfunction and vorticity fields: Results are presented for the 200 and the 1000 millibars surfaces, figures 7(a and b), respectively. The solid isopleths in these figures show the streamfunction

and the dashed isopleths show the distribution of absolute vorticity (units 10^{-6} sec^{-1}).

The streamfunction distribution at 200 mb contains one large anticyclonic circulation center in the northern Pacific Ocean and a center over northern Australia. Strong easterlies are found over the equatorial latitudes between these centers. At higher latitudes an upper troughs in the westerlies contain values of absolute vorticity $\approx 1 \times 10^{-4} \text{ sec}^{-1}$ in the Northern Hemisphere and $\approx -1 \times 10^{-4} \text{ sec}^{-1}$ in the Southern Hemisphere. The zero isopleth of absolute vorticity meanders across the equator. At the 1000 millibar surface a maximum value of absolute vorticity is found southeast of the Truk Islands in the northern Pacific Ocean. This is associated with a cyclonic disturbance along the western end of the asymptote of convergence. Observed wind directions and the streamfunction are nearly parallel at the 200 millibar surface, while they are not nearly so in the vicinity of the asymptote of convergence at the 1000 millibar surface. A stronger divergent component of wind was present at the lower level in the vicinity of the ITCZ. The cyclonic disturbances over the subtropical latitudes of the Southern Hemisphere are indicated by the large negative values of absolute vorticity.

f) Vertical Motions on top of the friction layer and calculated cloud cover: Figure 8 shows the isopleths of the initial balanced vertical motions $\times 10^{-5} \text{ mb/sec}$ at the 900 millibar surface (solid lines), while the calculated percent area of convective cloud cover is shown by dashed lines. The shaded region has some fraction of the synoptic scale grid (2° latitude \times 2° longitude) covered by convective clouds, and the unshaded region is free of convective clouds. The subtropical disturbances of the Southern Hemisphere exhibit marked convective cloudiness.

Maximum active cloud amounts range from 0.5 to 1 per cent in these disturbances. Balanced vertical motion in these disturbances has a maximum value $\approx -60 \times 10^{-5}$ mb/sec which is ≈ 1 cm/sec. The principal region of interest in this study is the surface asymptote of convergence. As stated earlier, the validity of the balanced vertical motions near the equator are questionable because Rossby number ≈ 1.0 .

A wide region of maximum rising motion (-60×10^{-5} mb/sec) with maximum cloud amounts ≈ 1 per cent is found in the vicinity of the ITCZ. Satellite cloud cover shows a narrow band of clouds, figure 6 (a and b), along 4°N near 170°E and a region with widespread convective activity between 140°E and 150°E . A region of sinking motion extends from 136°E to 152°E along the equator, this implies that air reaching the equator from the Southern Hemisphere is sinking at the rate of 1 cm/sec before it begins to ascend in the vicinity of the asymptote of convergence in the Northern Hemisphere. These calculations of cloud cover and the intensity of vertical motion appear somewhat unrealistic in the vicinity of the equator. Short-range prediction with this initial distribution of mass, motion and moisture variables reveals some interesting changes in the vicinity of the equator; this is discussed in the following section.

7. A discussion of the time evolution of various fields

Some of the results of the calculations will be discussed in this section.

a) 1000 and 200 millibar wind field at 24 hours:

Figures 9 (a and b), respectively, show these fields. The plotted winds are the observations at 24 hours, and the isopleths are the predicted

are extremely interesting. The wind field at 1000 millibars exhibits an east-west oriented asymptote of convergence. Convective activity is rather well marked along this asymptote of convergence. We felt that the forecasts after 30 hours were not very reliable, mainly because of boundary errors. The major asymptote of convergence and associated convective cloud band exhibits an equatorward movement. Convective activity weakens somewhat as the band moves from 4°N at 24 hours to near the equator. At 30 hours this system strengthens again and is located at 5°S at 48 hours of forecast time. Meanwhile a new asymptote of convergence forms at 12 to 16°N latitudes. Our calculations show that rather large changes can occur in the tropics during a 48-hour period. This is not surprising because satellite photographs, figure 6 (a and b), indicate marked changes in cloud cover. Manabe and Smagorinsky (1967) also mention that tropical disturbances have a rather variable structure during 1 to 3 day periods.

c) Vertical motions at 900 millibars (10^{-5} millibars/sec)

During the course of the time integration other relevant fields like convergence of mass between 1000 and 900 millibars, convergence of moisture between 1000 and 900 millibars and the net convergence of moisture between 1000 and 100 millibars were printed out at 6-hour intervals. It is true, that numerical models cannot be expected to reveal any more physics than what is already stated by the basic equations of our models. We did not impose any very direct relationships in our basic equations between the cloud cover computations and the various parameterization features listed above. We observed the following results of interest:

Asymptotes of convergence, percent cloud cover, upward vertical motions on top of friction layer and net moisture convergence all revealed rather similar patterns. Figure 11 (a,b,c,d) shows the friction layer vertical motions in 6-hour steps with superimposed 1000 millibar wind directions. Results at 18 and 24 hours again appeared very realistic. Largest vertical motions are of the order - 300×10^{-5} mb/sec, i.e. ≈ 4 cms rising motion.

The evolution of the vertical motion field in a vertical plane is shown in figure 12. The vertical plane is a north-south cross section from 28°N through 28°S at 152°E longitude. This plane intersects an active portion of the ITCZ. The field of vertical motion undergoes considerable adjustment in the first 18 hours in the equatorial latitudes. This field appears very realistic at 18 and 24 hours of forecast time. The largest magnitudes of vertical motion occur at 24 hours and are - 200×10^{-5} mb/sec (≈ 3 cm/sec) and + 500×10^{-5} mb/sec (≈ -7 cm/sec) in the mid troposphere. The adjustment of the vertical motion field produces a solution that is quite asimilar to initial vertical motions. Magnitudes of ω_{1000} are of the order of 25×10^{-5} mb/sec (vertical motion is zero at 100 millibars).

d) Some parameters related to parameterization of cumulus convection:

In figure 13 we show the time variation in 6-hour steps at 152°E and between 28°S and 28°N of the following quantities:

- i) Specific humidity at 900 mb (gm/kgm)
- ii) Percent cloud cover
- iii) Net moisture convergence (unit 10^{-8} mb meter $^{-1}$ sec).

The field of specific humidity changes very slightly during the first 24 hours. Along this section specific humidity varies between 10 and 18 gm/kgm between the equatorial maximum value and lower values near 28°N and 28°S . The region of maximum moisture is not the most convectively active region. Percent cloud cover (maximum 1 per cent) and the net moisture convergence are very nearly proportional to each other. These fields undergo rapid variations during the first 18 hours.

It appears from the nature of these variations that spurious vertical advections of heat and moisture take place during the adjustment process. For short-range predictions in low latitudes, it is highly desirable that such spurious effects be removed right from the start. Unfortunately, the present model is incapable of alleviating this problem. To the best of the author's knowledge, suppression of this initial oscillation has not been satisfactorily carried out in any real initial data experiments. Miyakoda and Moyer (1968) and Nitta and Hovermale (1967) have proposed procedures for initialization that could alleviate this difficulty, but because of limited tests in their studies, no general statement can be made at present.

e) An experiment with constant relative humidity on each pressure level at initial time:

As stated earlier, the initial moisture distribution is somewhat unreliable, hence relative humidity obtained from subjective analysis was averaged horizontally over the domain of integration in this experiment. Thus initially no gradients of relative humidity were present on constant pressure surfaces but it should be noted that specific humidity is not a constant. The results of numerical prediction of the mass and motion

fields at 24 hours were quite similar to those obtained from detailed analysis of moisture. This implies the following important feature of the parameterization of the cumulus scale in this experiment:

$$\nabla \cdot q \nabla W \approx q \nabla \cdot W, \text{ i.e. } W \cdot \nabla q$$

is small. Mass convergence is a more pronounced feature of the flows and accounts for the net convergence of flux of moisture while horizontal advection of moisture contributes less. This statement must be interpreted with some caution, because this is only true in a gross sense. The author has carried out another detailed synoptic study (Krishnamurti, 1968b) of various parameters of large-scale flows and their relation to convective cloud cover as revealed by radar returns over the Caribbean. It was found that mass convergence and moisture convergence were not of the same sign over all regions near 900 mb. Since the moisture variable is one of the most unreliable fields in our input we might suggest that a constant distribution of relative humidity on pressure surfaces might be a useful compromise for very short-range prediction.

8. Some comments on the dynamics of the intertropical convergence zone

The field of vertical motions in the balance initial state is in good agreement with the synoptic disturbances north of 15°N and south of 15°S. In the vicinity of the equator initial vertical motion field shows a general region of rising motion north of the surface asymptote of convergence and does not appear to be very realistic. A short range prediction in a matter of 18 to 24 hours yields a rather realistic pattern of rising motion that extends from east to west almost along

the asymptote of convergence in the surface forecast wind field. The initial discrepancy must be due to the inadequate dynamics of the balanced initial state which is only valid for flows characterized by a small Rossby number. The adjustment of the three-dimensional motion field to the temperature, moisture, mass field, and other external boundary parameters is interesting. A narrow axis of computed cloud cover at 24 hours along 4°N raises the question whether the output information at 24 hours could be used to investigate some aspects of the dynamics of the intertropical convergence zone. A short-range prediction is certainly not a simulation experiment, our initial data does already contain the proper ingredients in the motion, temperature and moisture variables to resolve in a matter of 24 hours a narrow region of cloud cover and rising motion along the asymptote of low-level convergence. At best, we could hope to merely carry out a diagnostic study with the detailed output information on tape at 24 hours. At this time there is some sort of a balance of the dependent variables for large Rossby number flows in the vicinity of the equator.

Diagnostic studies are generally limited in scope, if calculations are carried out in a small domain (as they are in our studies), any description of the local circulation can be somewhat biased. A pertinent question that could be raised at this point would be on the maintenance of the kinetic energy of the wind field.

Let us consider a box enclosing the region, 16°N through 16°S , 1000 millibars through 100 millibars and from 104°E through 128°W . Because of the imposed cyclic continuity there are no boundary fluxes in the zonal direction.

The following integrals, respectively, represent the conversions of zonal kinetic energy and eddy available potential energy into eddy kinetic energy, see Lorenz (1960), and Manabe and Smagorinsky (1967).

$$(K_Z \rightarrow K_E) = -\frac{1}{g} \int_{100}^{1000} \left(\overline{u'v'} \frac{\partial \bar{u}}{\partial y} + \bar{\omega}' \overline{u'} \frac{\partial \bar{u}}{\partial p} \right) dp \quad (45)$$

$$(P_E \rightarrow K_E) = -\frac{R}{g} \int_{100}^{1000} \left(\frac{\overline{\omega'T'}}{p} \right) dp \quad (46)$$

Equations (45) and (46) represent contributions to energy transformations at a fixed latitude, primes are departures from zonal averages and bar is a zonal average, other symbols are explained elsewhere.

The net energy conversion over the box may, if desired, be obtained by merely integrating these conversions over the surface area of the box. Both of these quantities may be expressed in millibar meter sec⁻¹ units. This unit seems more appropriate, because we are merely comparing the two rates of energy transfer with respect to each other. For similar calculations Manabe and Smagorinsky (1967) use Joule/(cm² day) as the unit, the conversion between these sets of units is 1 Joule/(cm² day) = ($\frac{1}{864}$) mb meter sec⁻¹.

Figure 14 shows the results of calculations at t = 24 hrs. In the vicinity of the intertropical convergence zone, the so-called barotropic conversion is a transfer from eddy to zonal kinetic energy while there is a stronger conversion of eddy potential to eddy kinetic energy. This result is not surprising if we examine the synoptic maps at different levels at t = 24 hours.

The wind field at 1000 and 200 millibars exhibits a belt of easterlies near the ITCZ. Easterlies are strong at low levels and at

higher levels, being quite variable and weak at the 600 and 400 millibar surfaces. At the lower level intense rising centers $\omega' < 0$ are found where $u' > 0$ (weaker easterlies near the ITCZ, see figure 15) in this region $\frac{\partial \bar{u}}{\partial p} < 0$. At higher levels $\omega' < 0$, $u' < 0$ and $\frac{\partial \bar{u}}{\partial p} > 0$. The net result of these configurations of the motion field yields

$$-\frac{1}{g} \int_{100}^{1000} \overline{\omega' u'} \frac{\partial \bar{u}}{\partial p} dp < 0.$$

Furthermore, along the asymptote of convergence lies a region of weak surface winds, figure 15. Just north of the ITCZ, along a latitude circle $v' < 0$, $u' > 0$, $\frac{\partial \bar{u}}{\partial y} < 0$, south of the ITCZ $v' > 0$, $u' > 0$, $\frac{\partial \bar{u}}{\partial y} > 0$, and hence

$$-\frac{1}{g} \int_{100}^{1000} \overline{u' v'} \frac{\partial \bar{u}}{\partial p} dp < 0.$$

Thus, the geometric configuration of the computed velocity field at 24 hours has a net barotropic energy exchange $(K_Z \cdot K_E) < 0$. This exchange is more than compensated by the ascending warm air $(P_E \cdot K_E)$ near the ITCZ, figure 11. The barotropic exchange away from the ITCZ shows $(K_Z \cdot K_E) > 0$ in both the Northern and Southern Hemispheres, this result is in accordance with Charney's (1963) scale analysis for large-scale motions in the tropics. The dominant energy conversion term is $(P_E \cdot K_E)$, though between $8^\circ S$ and $16^\circ S$ and between $8^\circ N$ and $16^\circ N$ $(K_Z \cdot K_E)$ is an appreciable fraction of the total exchange.

The intense rising motion (ω') along the ITCZ in our model is mainly attributable to the coupling of strong frictional convergence and the convective release of latent heat. An experiment was also performed without latent heat but including surface friction. The results indicated

a breakdown of the elongated asymptote of convergence into several large eddies in a matter of 18 hours. Perhaps this result was a consequence of improper energetics and the adjustment of our balance initial state to this situation.

Because of the limited nature of the present investigation, a complete energetics of an open system containing the ITCZ was not carried out.

10. Some concluding remarks:

The procedure for parameterization of cumulus convection used in this study is rather crude. Vertical momentum transfer in sub-grid scale motion is not included. Recently Ooyama (1967) and Estoque (1967) have considered this effect in their studies. Its inclusion would be a simple extension of the present study. We have shown that a somewhat realistic short-range prediction of larger scale flows in equatorial latitudes is not possible without a parameterisation of the cumulus scale. We have, however, made a tacit assumption that cumulus convection is always expressible as a function of larger-scale moisture convergence. This is generally the case, but it excludes the possibility of isolated cumulus convection with local smaller-scale mass compensation. Convection over heated islands and sea breeze effects generally occur without bearing any relationship to organized larger-scale mass or moisture convergence, though they may be modified by the prevailing synoptic situation. This is not, however, a hopeless problem. Parameterization of cumulus convection could, in principle, be carried out to include both of these effects separately. There is thus an obvious need for a detailed climatological investigation of cloudiness over all islands and coastal regions that are known to exhibit

local diurnal convection. If such statistics were accumulated over the entire tropics then this information could be introduced in some empirical manner into larger scale numerical prediction models. This is necessary because convective clouds, no matter how they are formed, do transfer large amounts of moisture, heat and momentum in the vertical direction and the larger-scale motions are gradually altered as a result. If a coarse mesh of the order of few hundred kilometers is used in prediction experiments then it may be important to include this second class of convective element. Parameterization of cumulus convection requires a knowledge of the distribution of moist unstable regions in the horizontal and in the vertical. A knowledge of the distribution of the moisture variable is thus quite important, yet we find that the initial analysis of this field is very difficult especially from the currently available data networks. Several massive research efforts in the tropics are currently being contemplated in the United States and other countries. It would be highly desirable to examine ways to obtain detailed three-dimensional distribution of moisture variables in low latitudes.

Some of the important results of the present study are as follows:

The dynamical structure of the tropical atmosphere in equatorial latitudes is poorly described by the balance model, but is reasonably well represented if a short-term numerical prediction is carried out.

At 24 hours of forecast time the following features are of interest. A well marked surface asymptote of convergence, the ITCZ, is found at 4°N . Along this asymptote an axis of frictional mass and moisture convergence is found with a maximum computed convective cloud cover. This study reveals a strong coupling between these three features. Along the

equator, sinking motion and absence of clouds is indicated by the computations. Furthermore we find that in the vicinity of the ITCZ, energy transformations show that $(P_E \cdot K_E)$ is positive, in agreement with the results of Manabe and Smagorinsky (1967) but we also find a surprising result that $(K_E \cdot K_Z)$ is positive. We have shown that the latter result is possible because of the detailed structure of wind field in low latitudes. Away from the ITCZ we find that $(K_Z \cdot K_E)$ is positive implying a barotropic instability of the zonal current. This study has demonstrated a limited success in short-range numerical prediction from real initial data in low latitudes.

Besides the difficulties of the parameterization of the cumulus scale other major defects of this study are related to lack of observations, contamination of forecasts due to lateral boundary conditions and the presence of gravity inertio-oscillations during the initial phase of the forecast period. Further work is continuing to examine in detail some of these problems.

Acknowledgements

Mr. Edward B. Rodgers, a graduate student at Florida State University, provided considerable assistance in data processing and analysis. Initial financial support for this work was provided by Air Force Cambridge Research Laboratories, Grant No. MIPR ES-7-967, while the author was at Naval Postgraduate School, Monterey, California. This work is being continued under support by the Atmospheric Science Section, National Science Foundation, NSF Grant GA-1480, at Florida State University. Computations were carried out on the IBM 7094 computer at the University of California and on the CDC 6400 computer at Florida State University.

REFERENCES

- Baumhefner, D. P. 1968 'Application of a diagnostic Numerical Model to the Tropical Atmosphere,' Mon. Wea. Rev., 96, pp. 218-228.
- Benwell, G. R. R. and 1968 'A pressure oscillation in a 10-level
Bretherton, F. P. atmospheric model,' Quart. J. R. Met. Soc., 94, pp. 123-131.
- Berkofsky, L. and 1960 'Topographic charts at one degree inter-
Bertoni, E. A. section for the entire earth,' G.R.D. Research Notes.No. 42, pp. 1-43, Air Force Cambridge Research Laboratories, Bedford, Mass.
- Bushby, F. H. and 1967 'A ten-level atmospheric model and frontal
Timpson, M. S. rain,' Quart. J. R. Met. Soc., 93, pp. 1-17.
- Charney, J. 1955 'The use of primitive equations of motion
in numerical prediction,' Tellus, 7, pp. 22-26.
- 1963 'A note on large-scale motions in the tropics,'
J. Atmos. Sci., 20, pp. 607-609.
- Charney, J. G. and 1964 'On the growth of the hurricane depression,'
Eliassen, A. J. Atmos. Sci., 21, pp. 68-75.
- Dean, G. A. 1956 'The 1955 mean monthly wind circulation over
the tropical central Pacific area,'
Institute of Geophysics, University of California, 16 pp.
- Elsasser, H. W. 1968 'Diagnosis of early baroclinic NWP models,'
J. Appl. Met., 7, pp. 153-159.
- Estoque, M. A. 1967 'Exchange processes due to penetrative
convection,' Bull. Amer. Met. Soc., 48, p. 624.
- Grammeltvedt, A. 1968 'A survey of finite difference schemes for
the primitive equations for a barotropic
fluid,' Technical Report, National Center
for Atmospheric Research, Boulder, Colorado.
- Gray, W. M. 1967 'Global view of the origin of tropical dis-
turbances and storms,' Atmospheric Science
Paper No. 114, Colorado State University,
Fort Collins, Colorado.

- Hawkins, H. E. and Rosenthal, S. L. 1965 'On the computation of the streamfunction from the wind field,' Mon. Wea. Rev., 93, pp. 245-252.
- Hinklemann, K. 1951 'Der Mechanismus des meteorologischen Lärmes,' Tellus, 3, pp. 285-296.
- Jacobs, W. C. 1951 'Large scale aspects of energy transformations over the oceans,' Compendium of Meteorology, American Meteorological Society, Boston, Mass.
- Krishnamurti, T. N. 1962 'Numerical integration of primitive equations by a quasi-lagrangian advective scheme,' J. Appl. Met., 1, pp. 508-521.
- 1968a 'A diagnostic balance model for studies of weather systems of low and high latitudes, Rossby number less than 1,' Mon. Wea. Rev., 96, pp. 197-207.
- 1968b 'A calculation of the percent area covered by convective clouds from moisture convergence,' J. Appl. Met., 7, pp. 184-195.
- Kuo, H. L. 1961 'Convection in conditionally unstable atmosphere,' Tellus, 13, pp. 441-459.
- 1965 'On formation and intensification of tropical cyclones through latent heat release by cumulus convection,' J. Atm. Sci., 22, pp. 40-63.
- Leith, C. 1964 'Lagrangian advection in an atmospheric model,' Tech. Note No. 66, pp. 168-176, World Met. Organiz., Geneva, Switzerland.
- Lilly, D. K. 1965 'On the computational stability of numerical solutions of time dependent non-linear geophysical fluid dynamics problems,' Mon. Wea. Rev., 93, pp. 11-26.
- Lorenz, E. N. 1960 'Energy and numerical weather prediction,' Tellus, 12, pp. 364-373.
- Manabe, S. and Smagorinsky, J. 1967 'Simulated climatology of a general circulation model with a hydrologic cycle II: Analysis of the tropical atmosphere,' Mon. Wea. Rev., 95, pp. 155-169.
- Matsuno, T. 1966a 'Quasi geostrophic motion in the equatorial area,' J. Met. Soc. Japan., 44, pp. 25-43.

- Matsuno, T. 1966b 'A finite difference scheme for time integrations of oscillatory equations with second order accuracy and sharp cut-off for high frequencies,' J. Met. Soc. Japan, 44, pp. 85-88.
- Mintz, Y. 1964 'Very long-term global integration of the primitive equations of atmospheric motion,' Technical Note No. 66, pp. 141-167, World Meteorological Organization, Geneva, Switzerland.
- Miyakoda, K. and Moyer, R. W. 1968 'A method of initialization for dynamical weather forecasting,' Tellus, 20, pp. 113-128.
- Miyakoda, K., Smagorinsky J., Strickles, R. F. and Hembree, G. D. 1968 'Experimental extended predictions with a nine level hemispheric model.' Technical Report, U.S. Department of Commerce, pp. 1-53, ESSA, Washington, D. C.
- Morskoi Atlas 1953 Russian Marine Atlas, Vol. II, Plates 1-85.
- Nitta T. and Hoverwale, J. B. 1967 'On analysis and initialization for the primitive forecast equations,' Weather Bureau Technical Memorandum No. NMC, 42, pp. 1-38. National Meteorological Center, Suitland, Maryland.
- Økland, H. 1965 'An experiment in cyclogenesis prediction by a two-level model,' Mon. Wea. Rev., 93, pp. 663-672.
- Ooyama, K. 1963 'A dynamical model for the study of tropical cyclone development,' Dept. of Meteorology and Oceanography, New York University, 26 pp.
- 1967 'Numerical simulation of the life cycle of tropical cyclones,' NSF Report No. GA-623, New York University, University Height, New York.
- Phillips, N. A. 1956 'The general circulation of the atmosphere, a numerical experiment,' Quart. J. R. Met. Soc., 82, pp. 123-164.
- 1960 'On the problem of initial data for primitive equations,' Tellus, 12, pp. 121-126.
- Riehl, H. 1945 Tropical Meteorology, McGraw-Hill Book Co., New York.

- Rohwer, C. 1931 'Evaporation from free water surfaces,' U.S. Dept. Agriculture, Technical Bulletin No. 217, 96 pp., Washington.
- Rosenthal, S. L. 1965 'Some preliminary theoretical considerations of tropospheric wave motions in equatorial latitudes,' Mon. Wea. Rev., 93, pp. 605-612.
- Sadler, J. C. 1967 'The tropical upper tropospheric trough as a secondary source of typhoons and a primary source of tradewind disturbances,' Final Report, No. AFCRL-67-0203, pp. 1-48, University of Hawaii, Institute of Geophys. to AFCRL, Bedford, Mass.
- Shuman, F. G. and 1968 'An operational six layer primitive equation
Hovermale, J. B. model,' J. Appl. Met., 7, (to be published).
- Smagorinsky, J. and 1965 'Prediction experiments with a general circula-
Staff Members tion model,' Proceedings of the Interna-
tional Symposium on Dynamics of Large Scale
Processes in the Atmosphere, pp. 23-30,
Moscow, USSR.
- U.S. Bureau of 1962 'Monthly mean charts, sea surface temperature,
Commercial North Pacific,' U.S. Fish Wildlife Service,
Fisheries Circular No. 134, Biological Laboratory,
Stanford, California.
- Webb, K. E. 1960 'An investigation of the evaporation from
Lake Eucumbene,' Technical Paper No. 10.
1-75 pp. Commonwealth Scientific and
Industrial Research Organization, Australia,
Division of Meteorology and Physics,
Melbourne, Australia.
- Yanai, M. 1961 'A detailed analysis of typhoon formation,'
J. Met. Soc. Japan, 39, pp. 187-214.

Figure Captions

Figure 1. Sketch of nine points on a pressure surface used in quasi-Lagrangian advection. P is the origin of a parcel at time $t - \Delta t$, and Q is a grid point where parcel arrives at time t.

Figure 2. Vertical staggering of variables in the initialization and prediction phase.

Figure 3. Procedure used for the parameterization of cumulus convection.

Figure 4. (a) (top) Streamlines (solid lines) and isotachs (dashed lines, knots) for March 1, 1965, 1200Z, at 1000 millibars, $t = 0$ in our experiment.

(b) (bottom) Streamlines (solid lines) and isotachs (dashed lines, knots) for March 1, 1965, 1200Z, at 200 millibars, $t = 0$ in our experiment.

Figure 5. (a) (top) Specific humidity distribution at 900 millibars, units gm/kgm, for March 1, 1965, 1200Z, $t = 0$ in our experiment.

(b) (bottom) Temperature distribution at 500 millibars, units $^{\circ}\text{A}$, for March 1, 1965, 1200Z, $t = 0$ in our experiment.

Figure 6. (a) (top) Satellite mosaics for March 1, 2 and 3, 1965, in the vicinity of 140°E longitude.

(b) (bottom) Satellite mosaics for March 1, 2 and 3, 1965, in the vicinity of 170°E longitude.

Figure 7. (a) (top) Initial streamfunction at 200 millibar surface, units $10^5 \text{ meter}^2 \text{ sec}^{-1}$, March 1, 1965, 1200Z.

(b) (bottom) Initial stream function at 1000-millibar surface, units $10^5 \text{ meter}^2 \text{ sec}^{-1}$, March 1, 1965, 1200Z.

Figure 8. Initial balance vertical motions (solid lines) at 900 millibar units $10^5 \text{ millibar/sec}$. The initial calculated percent convective cloud cover is shown by dashed lines and this region is shaded. March 1, 1965, 1200Z.

Figure 9. (a) (top) 24-hour forecast of the wind field at 1000 millibars, solid lines are streamlines and dashed lines are isotachs in knots. The plotted winds are observations at verification time, i.e. March 2, 1965, 1200Z.

(b) (bottom) Same as figure 9(a) except at 200 millibars.

Figure 10. (a, b, c and d) 6-, 12-, 18- and 24-hour forecast of the distribution of percent area of convective cloud cover, shaded region. The wind arrows are the directions of the forecast wind vectors at the 1000 mb surface.

Figure 11. (a, b, c and d) 6-, 12-, 18- and 24-hour forecast of the distributions of 900-millibar vertical motions, units $10^{-5} \text{ millibar/sec}$, the shaded region indicates rising motions. The wind arrows are the directions of the forecast wind vectors at the 1000 mb surface.

Fig. 12. Vertical cross-section of vertical motion (10^{-5} millibar/sec) at 6, 12, 18 and 24 hours of forecast time. This cross section is taken in a south-north plane at 152°W longitude, and it intersects the ITCZ.

Figure 13. Time variation (along ordinate) of selected parameters at 152°W from south to north (along abscissa).

q specific humidity at 900 mb gm/kgm

a percent cloud cover

I net moisture convergence (10^{-8} mb meter $^{-1}$ sec).

Figure 14. Selected energy conversions at $t = 24$ hours of forecast time, evaluated from equations (45) and (46) of text.

Figure 15. An enlarged view of the 1000 mb, 24-hour forecast of wind directions (arrows) and wind speeds (knots, solid lines) in the vicinity of the ITCZ (heavy dark line).

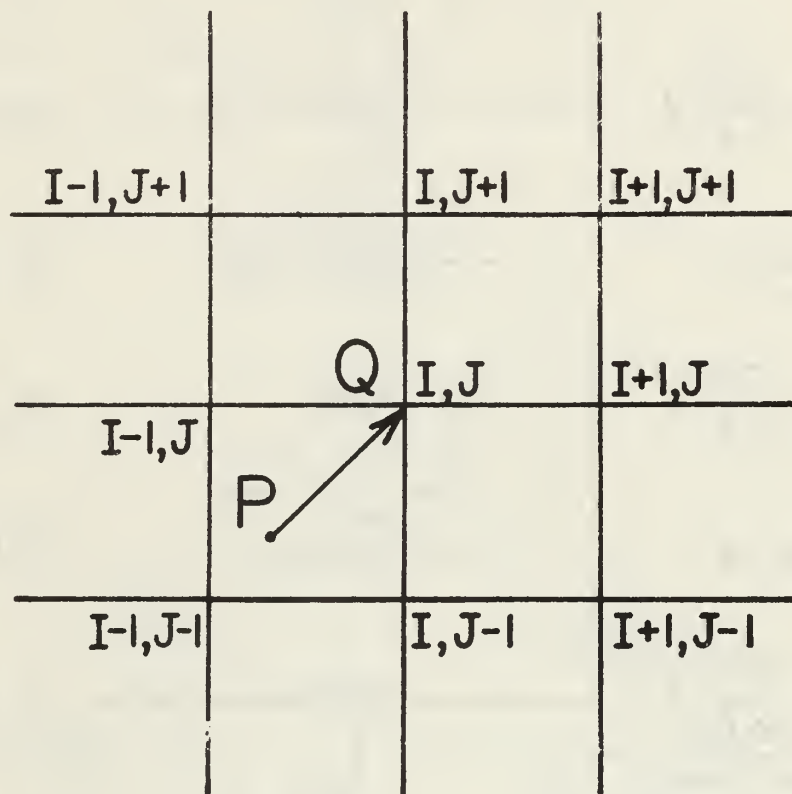
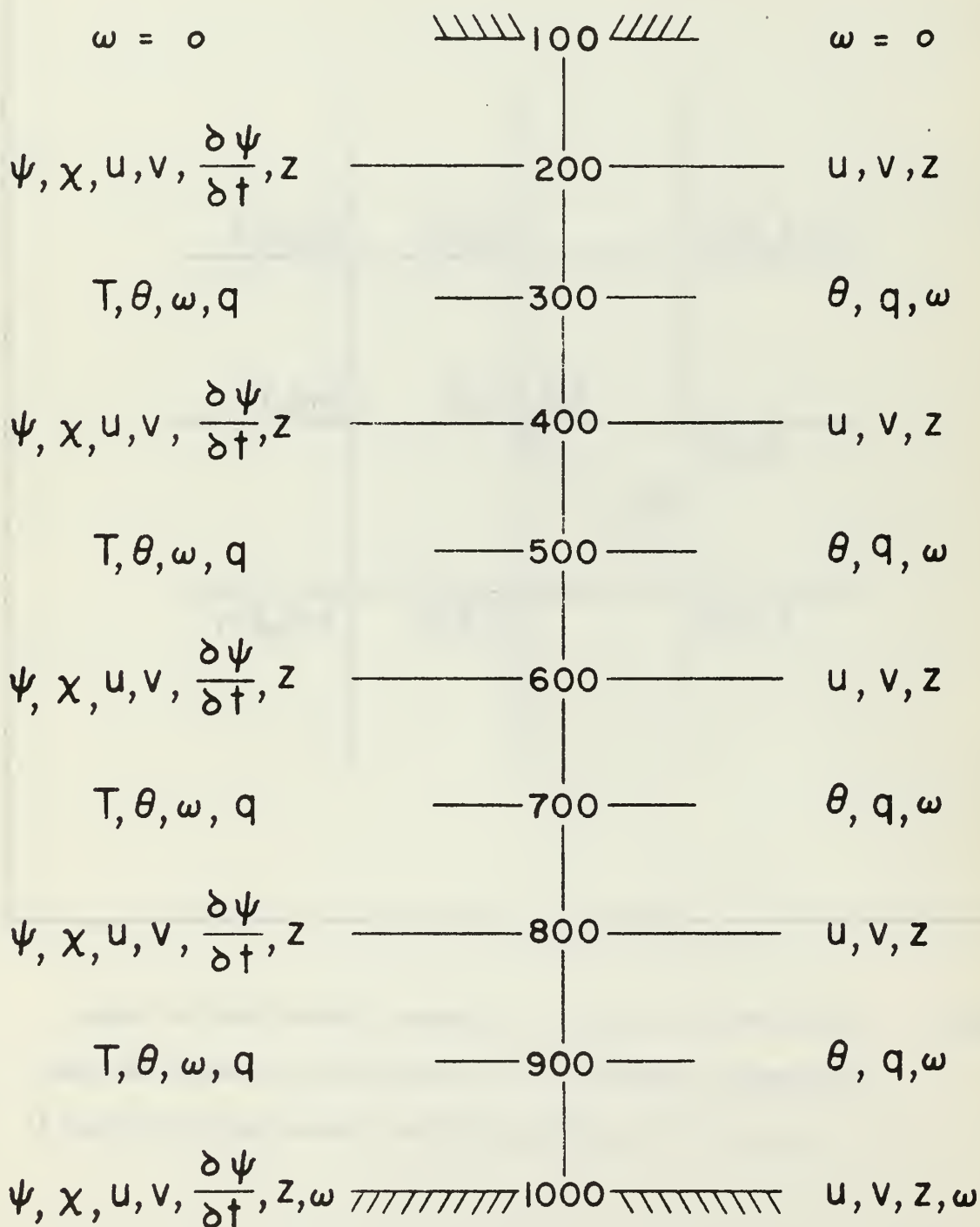


Figure 1. Sketch of nine points on a pressure surface used in quasi-Lagrangian advection. P is the origin of a parcel at time $t - \Delta t$, and Q is a grid point where parcel arrives at time t .

$t=0$ BALANCE EQUATION

$t>0$ PRIMITIVE EQUATION



VERTICAL PRESSURE LEVELS AND STAGGERING OF VARIABLES

Figure 2. Vertical staggering of variables in the initialization and prediction phase.

FLOW CHART FOR CUMULUS SCALE HEATING:-

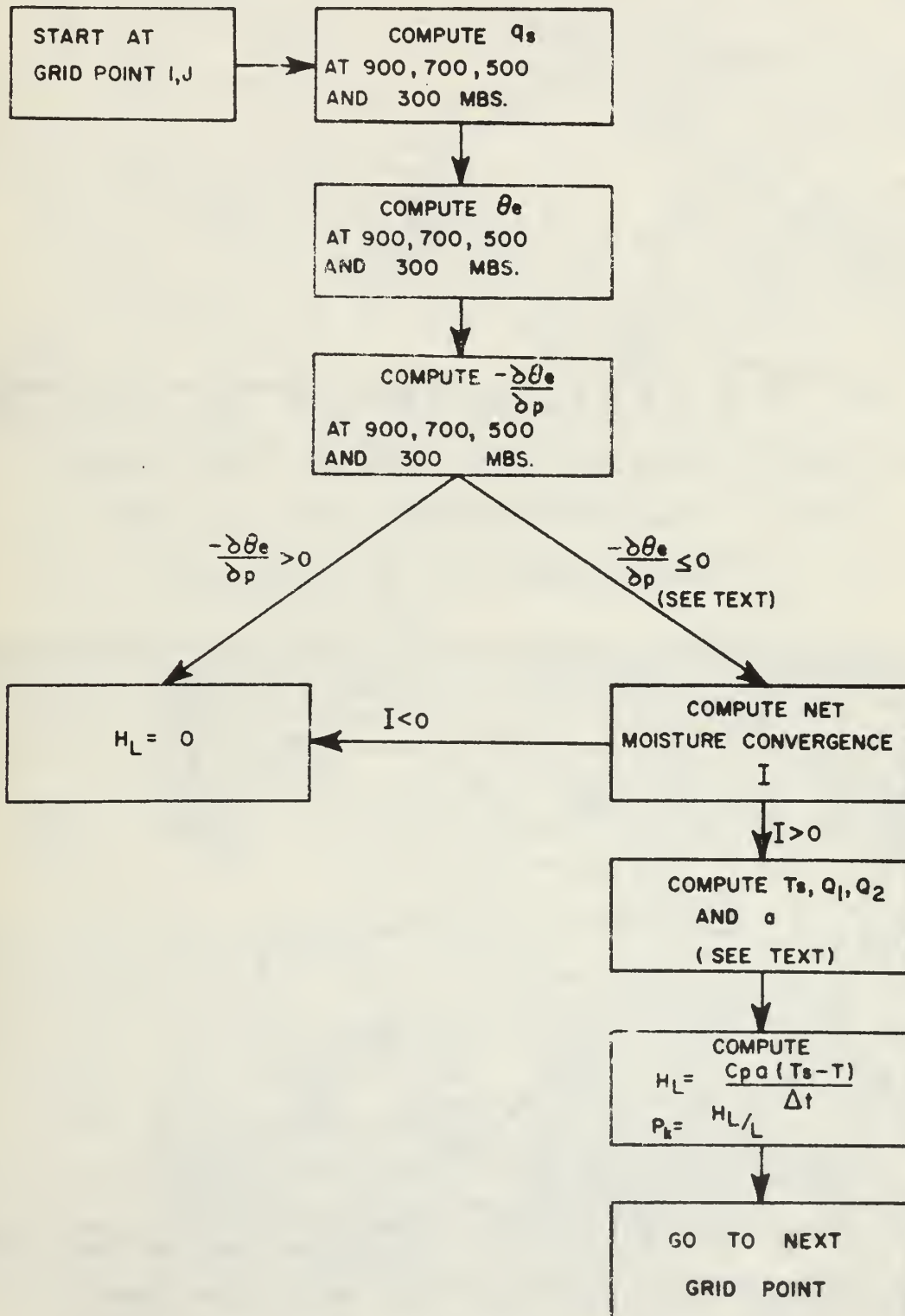


Figure 3. Procedure used for the parameterization of cumulus convection.

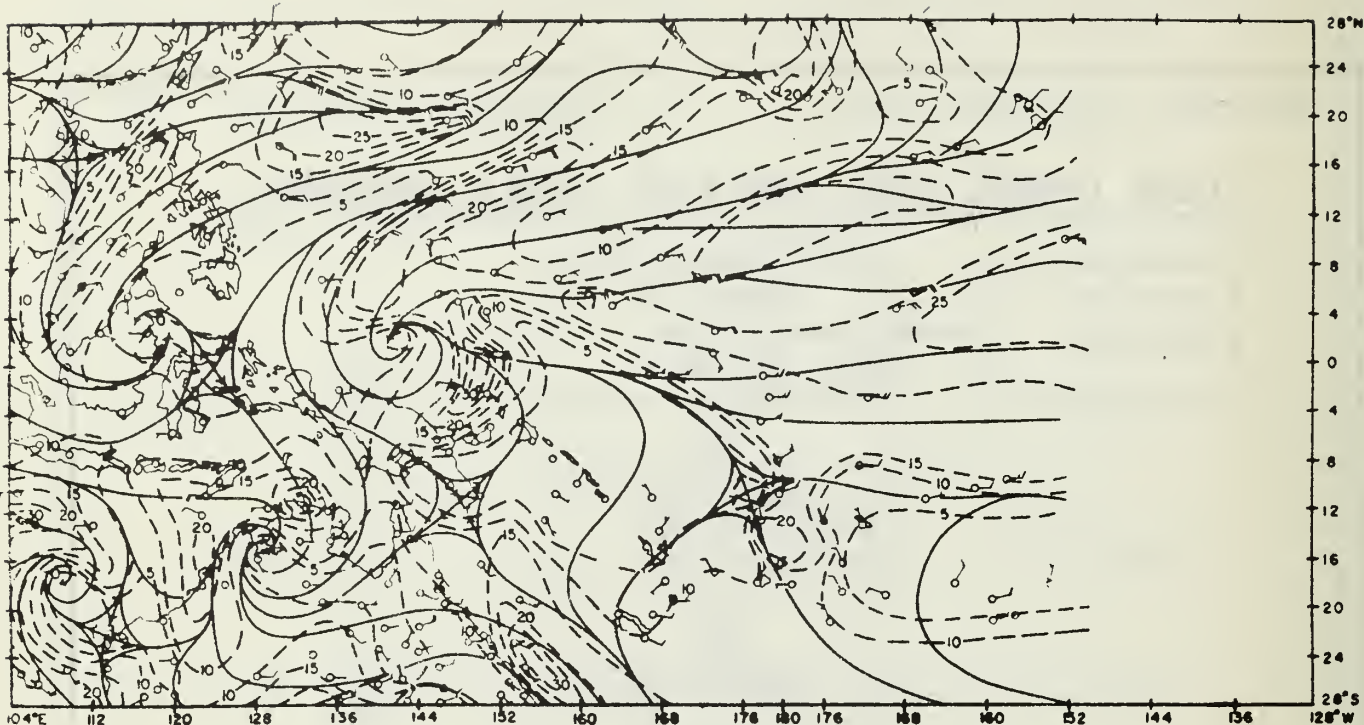
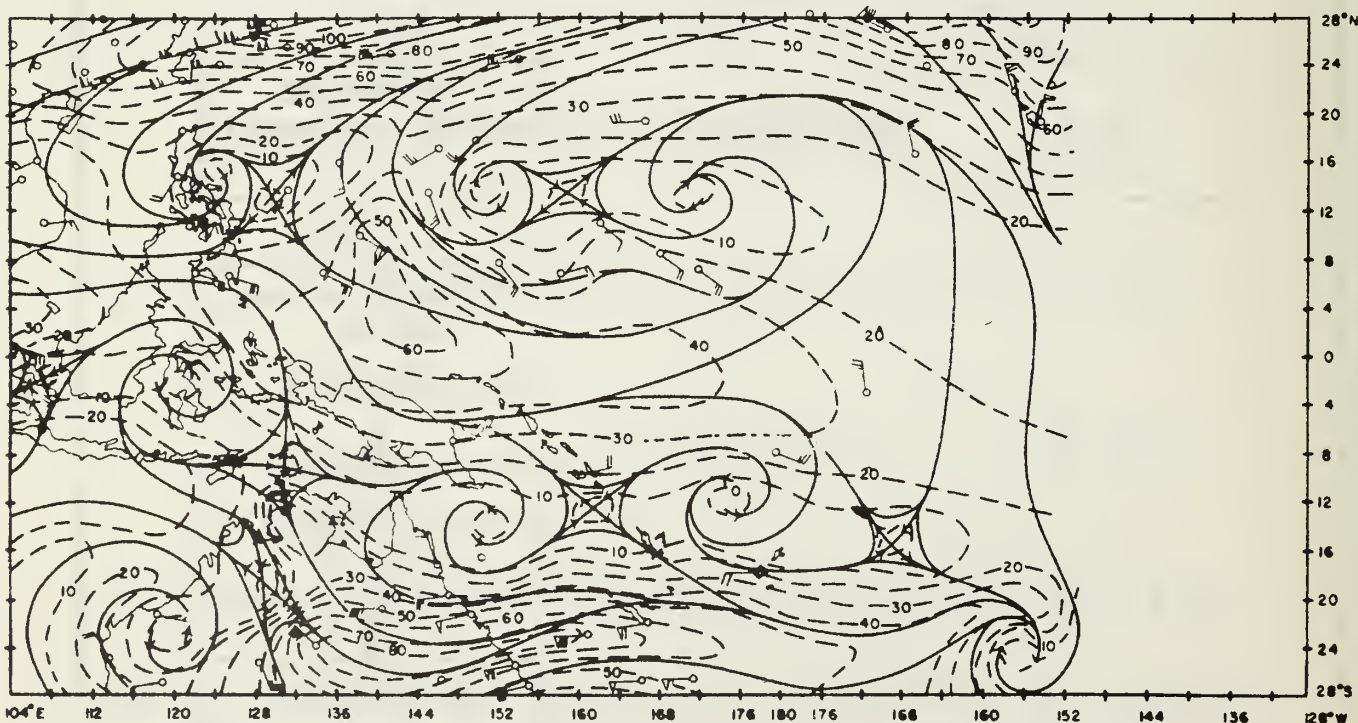


Figure 4. (a) (top) Streamlines (solid lines) and isotachs (dashed lines, knots) for March 1, 1965, 1200Z, at 1000 millibars, $t = 0$ in our experiment.



(b) (bottom) Streamlines (solid lines) and isotachs (dashed lines, knots) for March 1, 1965, 1200Z, at 200 millibars, $t = 0$ in our experiment.

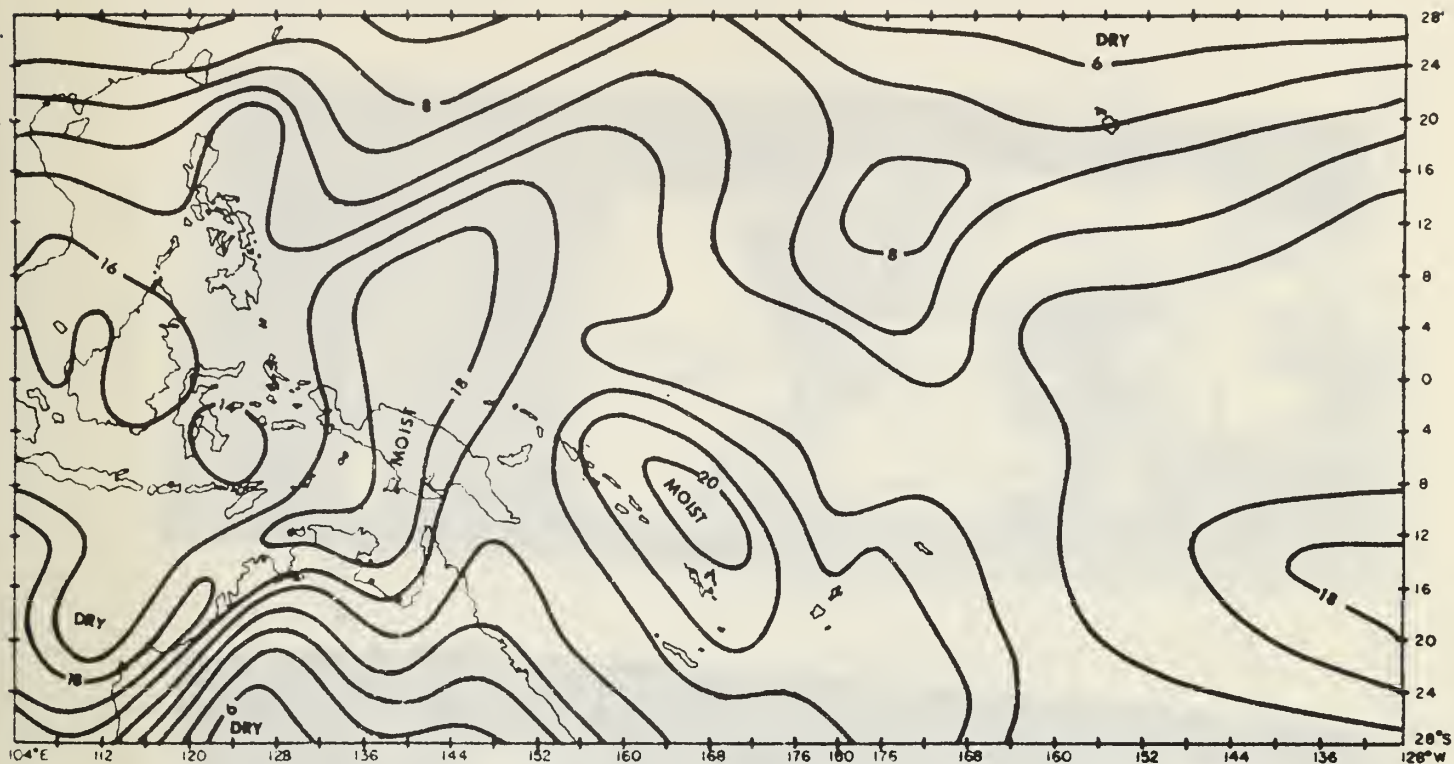
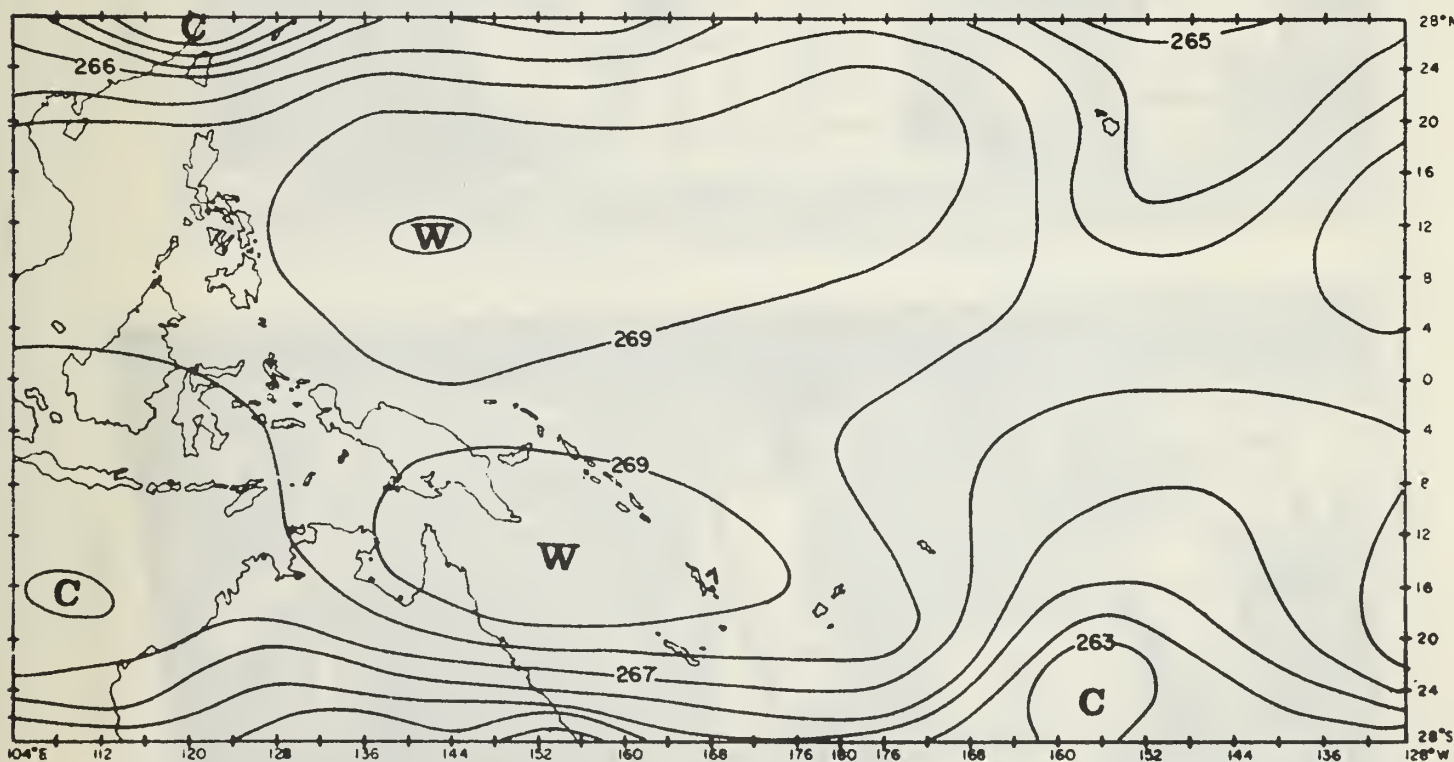


Figure 5. (a) (top) Specific humidity distribution at 900 millibars, units gm/kgm, for March 1, 1965, 1200Z, $t = 0$ in our experiment.



(b) (bottom) Temperature distribution at 500 millibars, units °A, for March 1, 1965, 1200Z, $t = 0$ in our experiment.

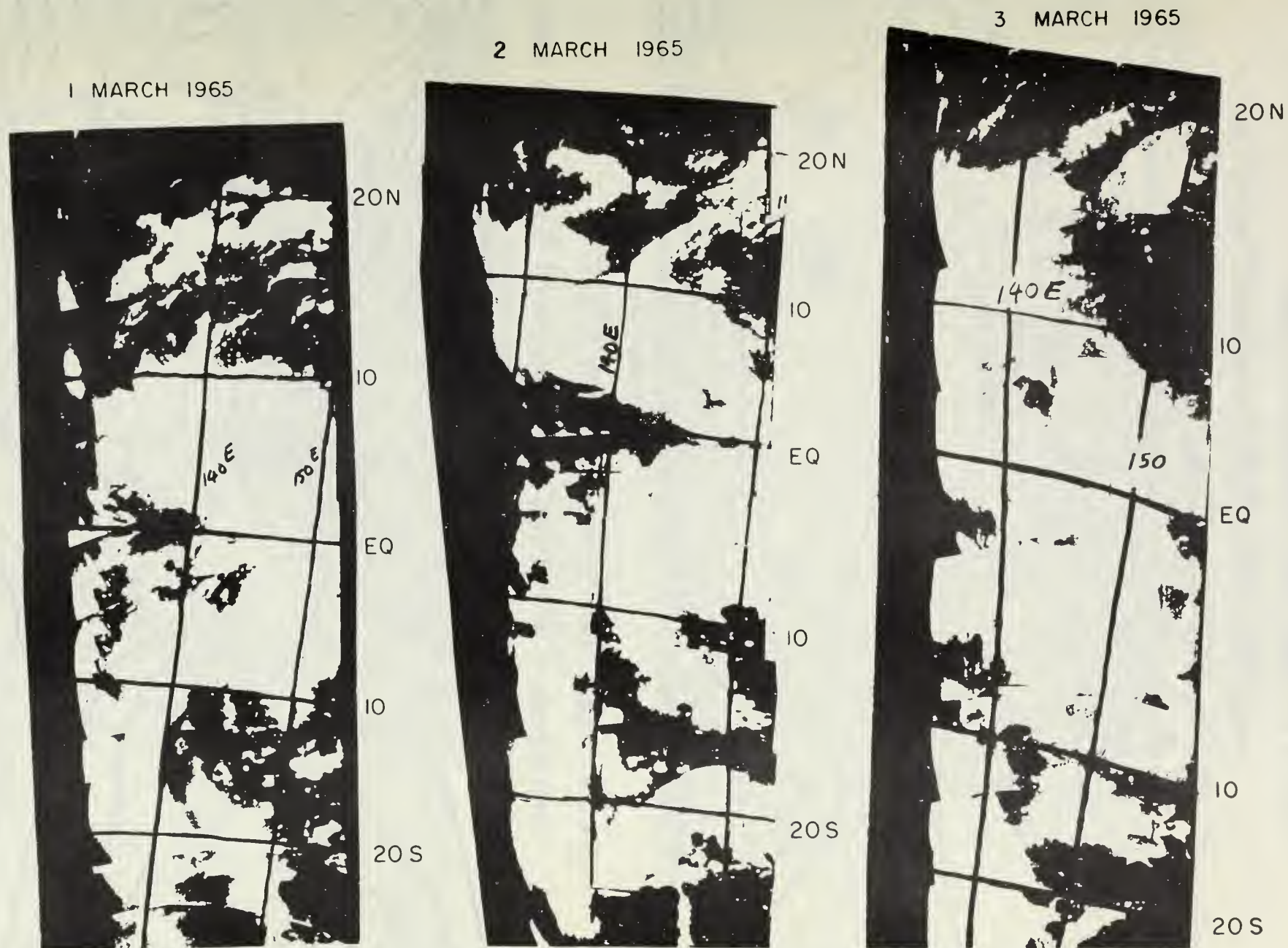
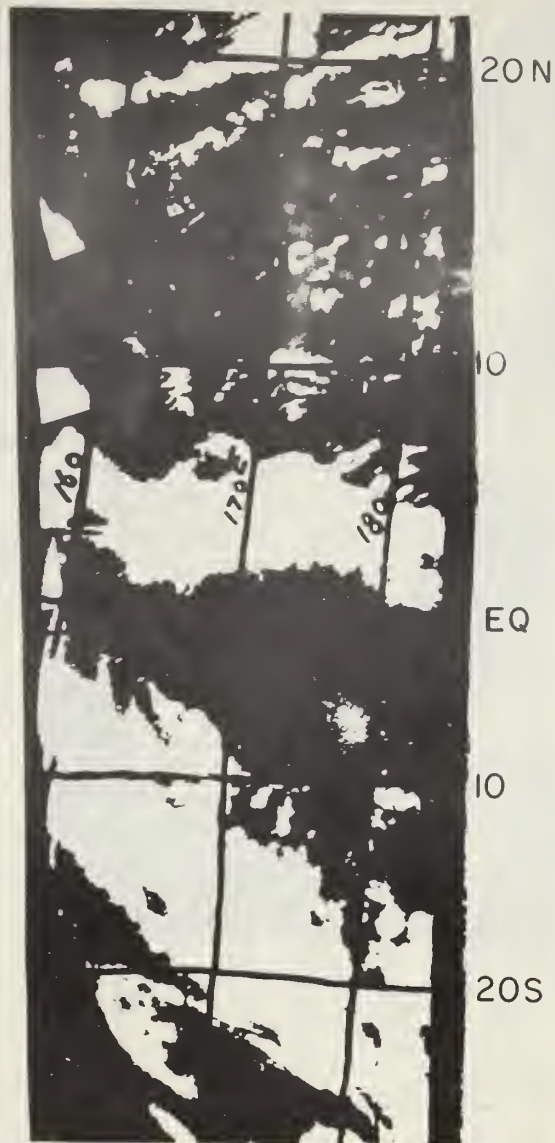
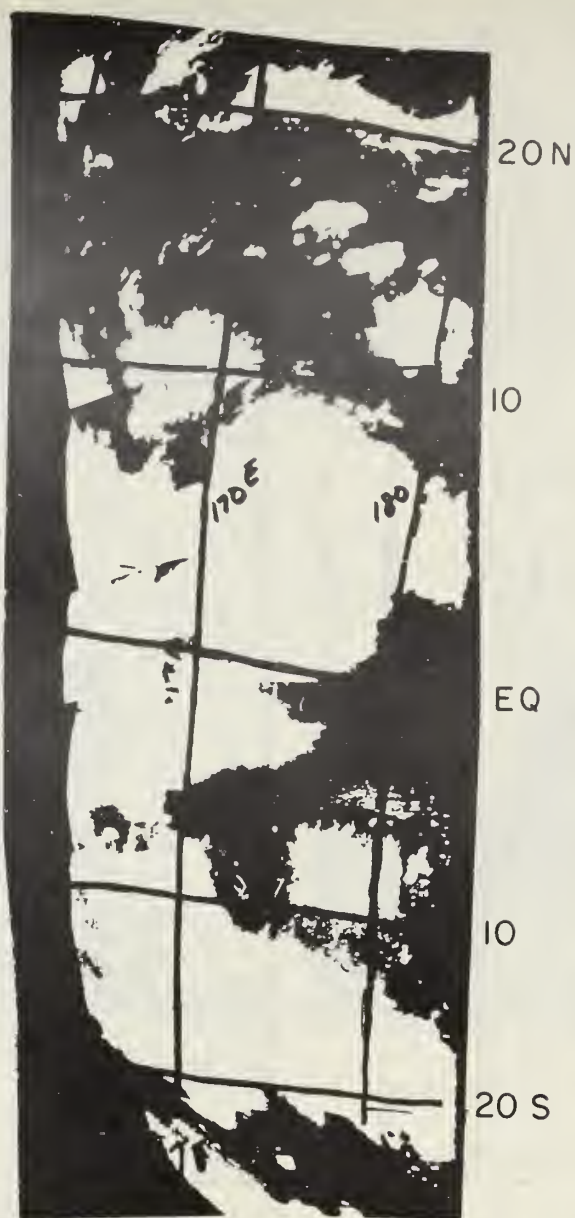


Figure 6. (a) Satellite mosaics for March 1, 2, and 3, 1965 in vicinity of 140°E longitude.

1 MARCH 1965



2 MARCH 1965



3 MARCH 1965

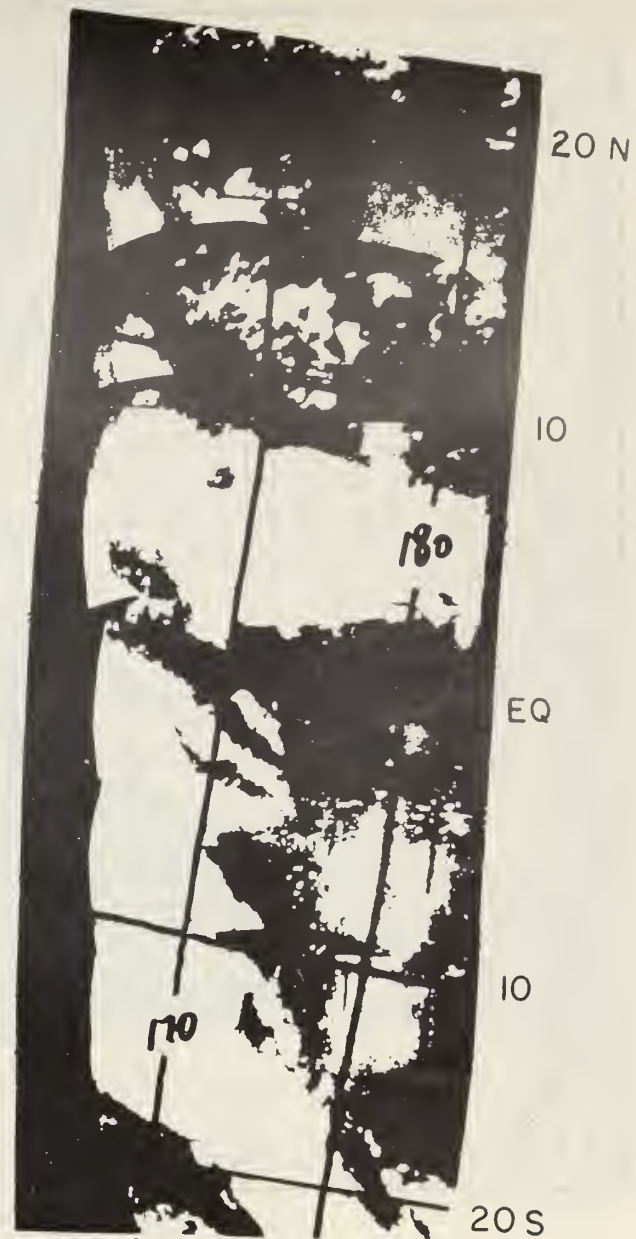


Figure 6. (b) Satellite mosaics for March 1, 2, and 3, 1965 in vicinity of 170°E longitude.

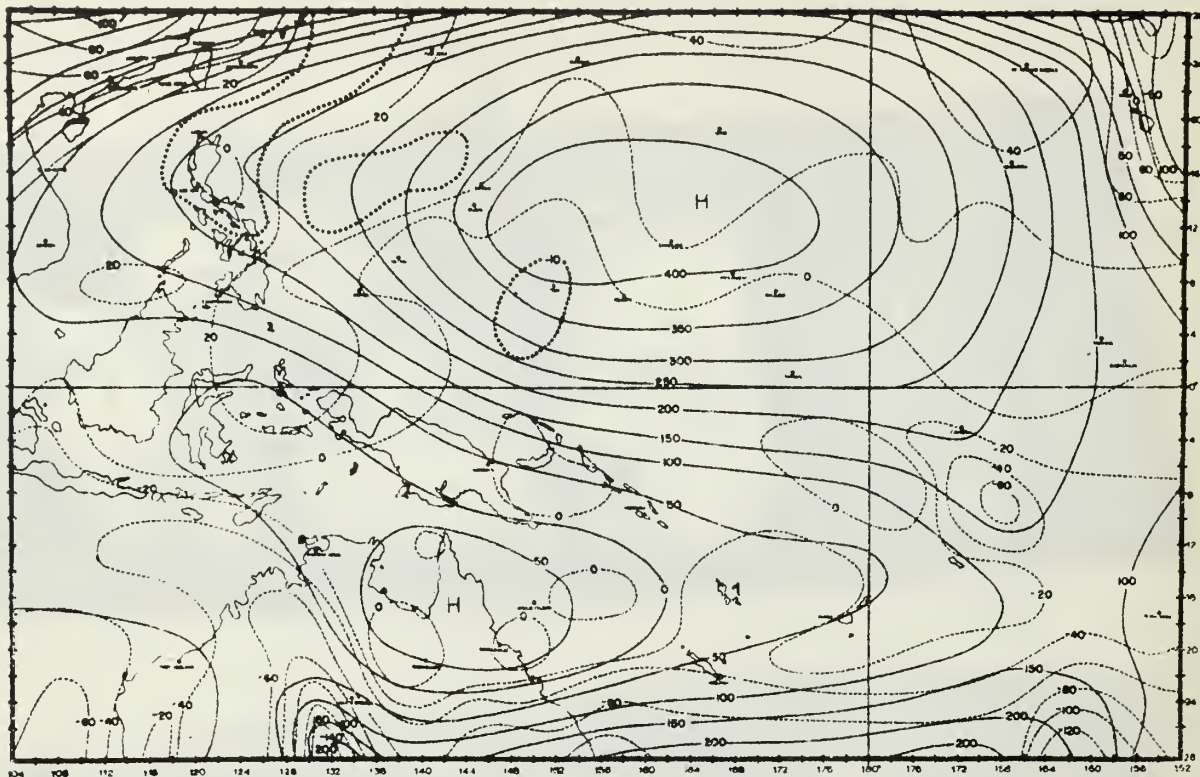
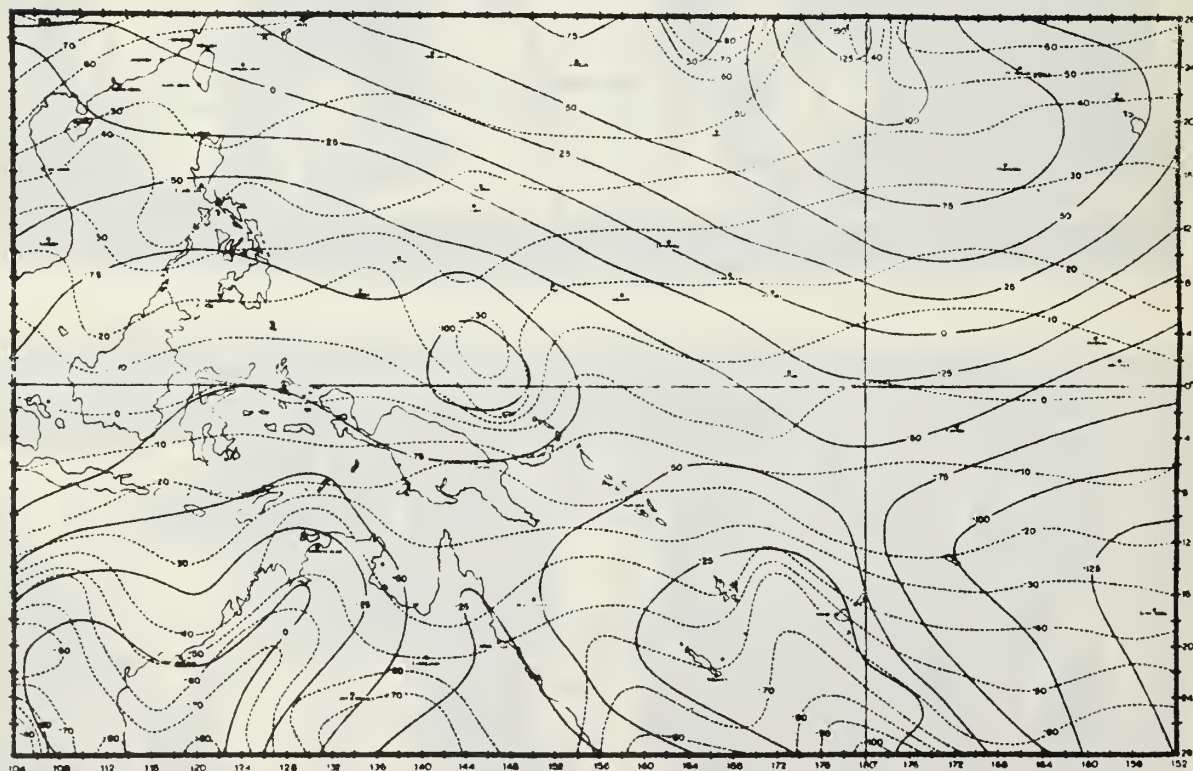


Figure 7. (a) (top) Initial streamfunction at 200 millibar surface, units $10^5 \text{ meter}^2 \text{ sec}^{-1}$, March 1, 1965, 1200Z.



(b) (bottom) Initial stream function at 1000-millibar surface, units $10^5 \text{ meter}^2 \text{ sec}^{-1}$, March 1, 1965, 1200Z.

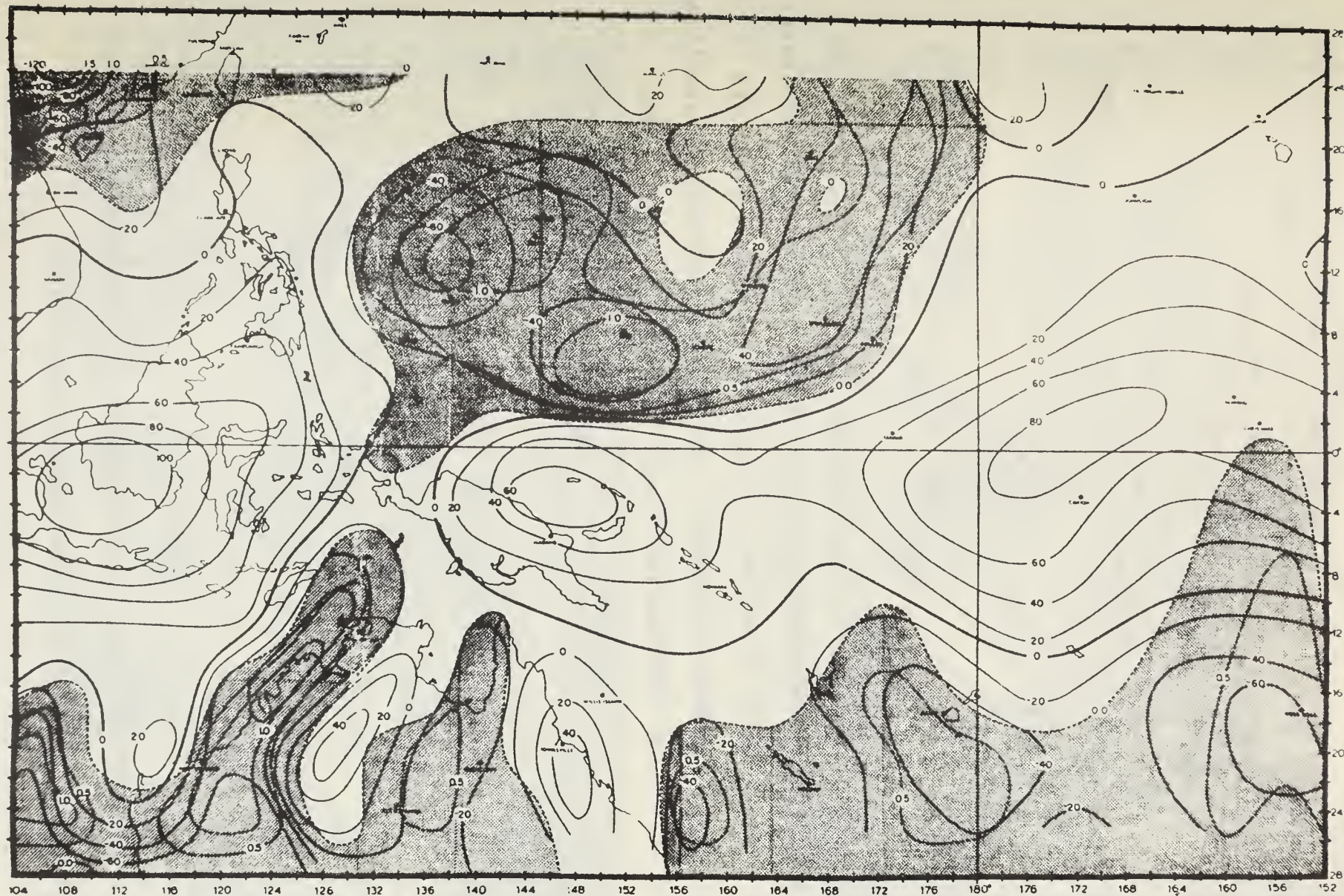


Figure 8. Initial balance vertical motions (solid lines) at 900 millibar units 10^5 millibar/sec. The initial calculated percent convective cloud cover is shown by dashed lines and this region is shaded. March 1, 1965, 1200Z.

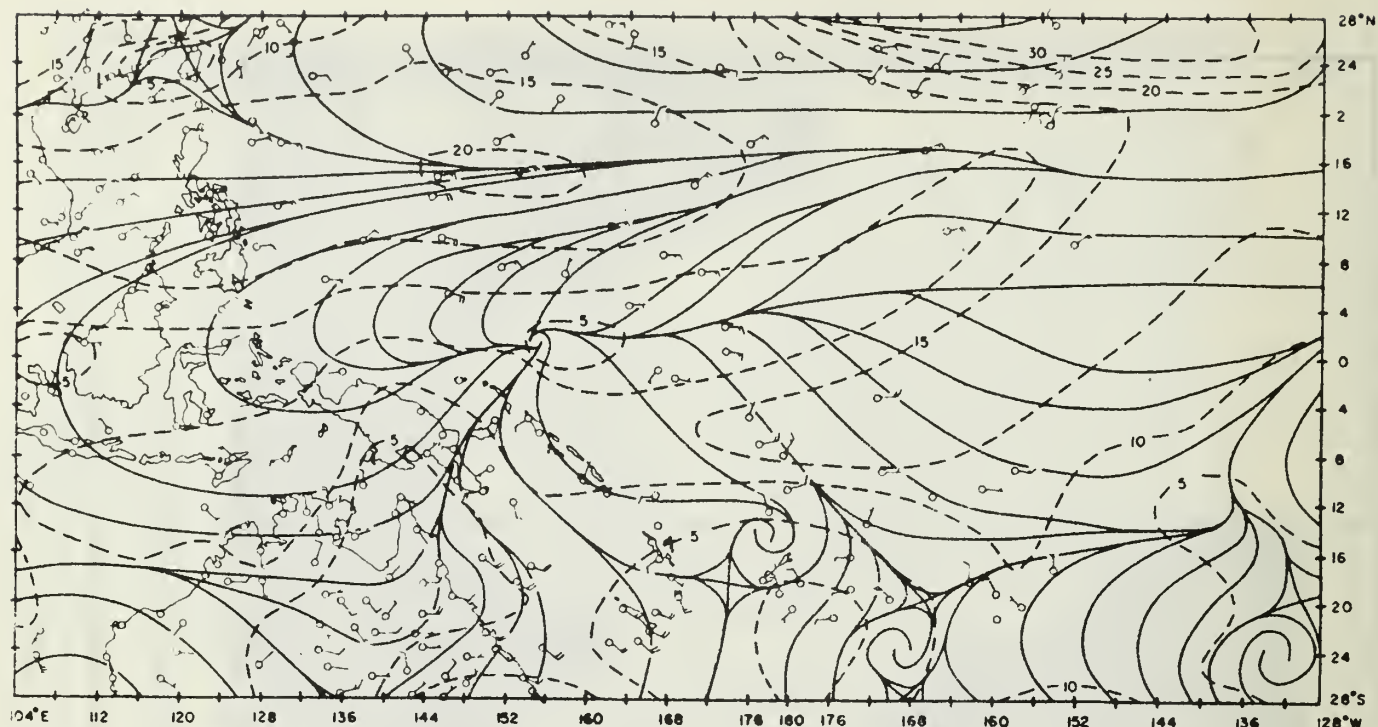
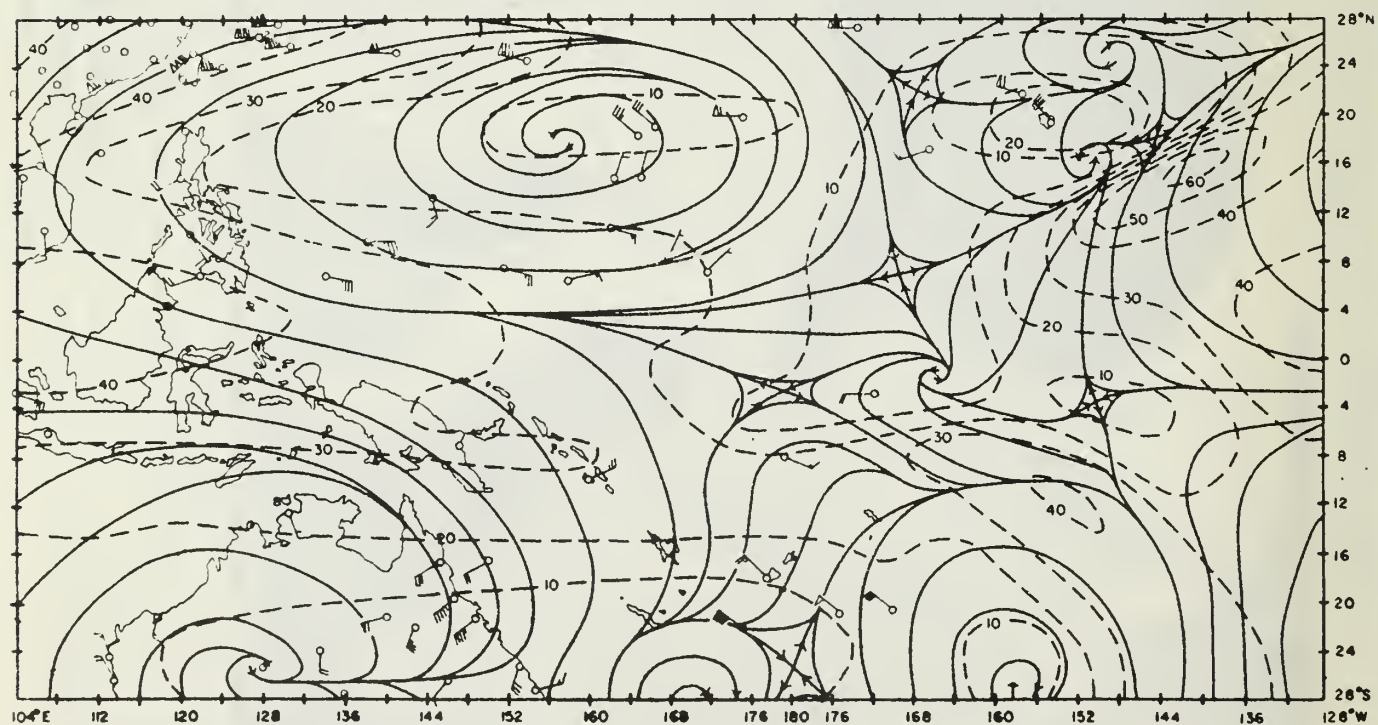


Figure 9. (a) (top) 24-hour forecast of the wind field at 1000 millibars, solid lines are streamlines and dashed lines are isotachs in knots. The plotted winds are observations at verification time, i.e. March 2, 1965, 1200Z.



(b) (bottom) Same as figure 9(a) except at 200 millibars.



Figure 10. (a, b, c, & d) 6-, 12, 18, and 24-hour forecast of the distribution of percent area of convective cloud cover, shaded region. The wind arrows are the directions of the forecast wind vectors at the 1000 mb surface.

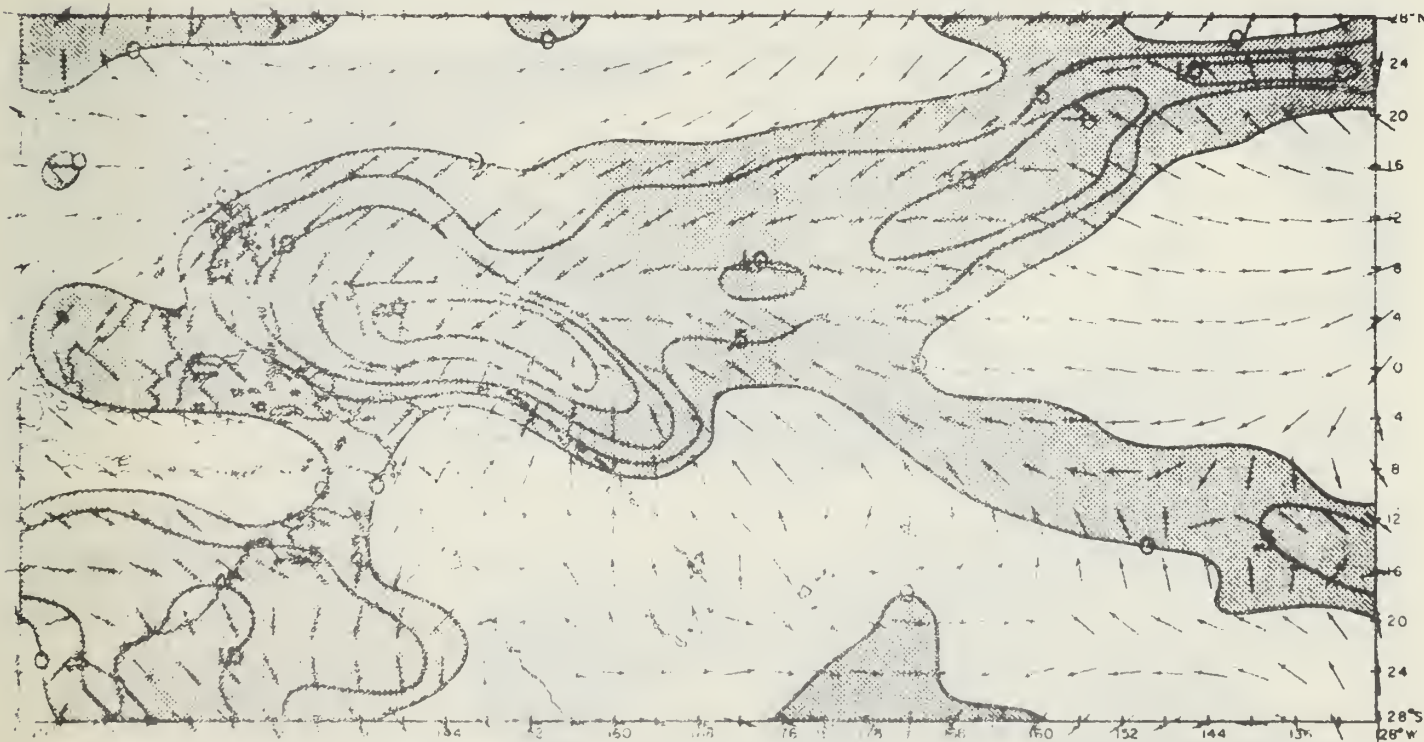


Figure 10. (b)

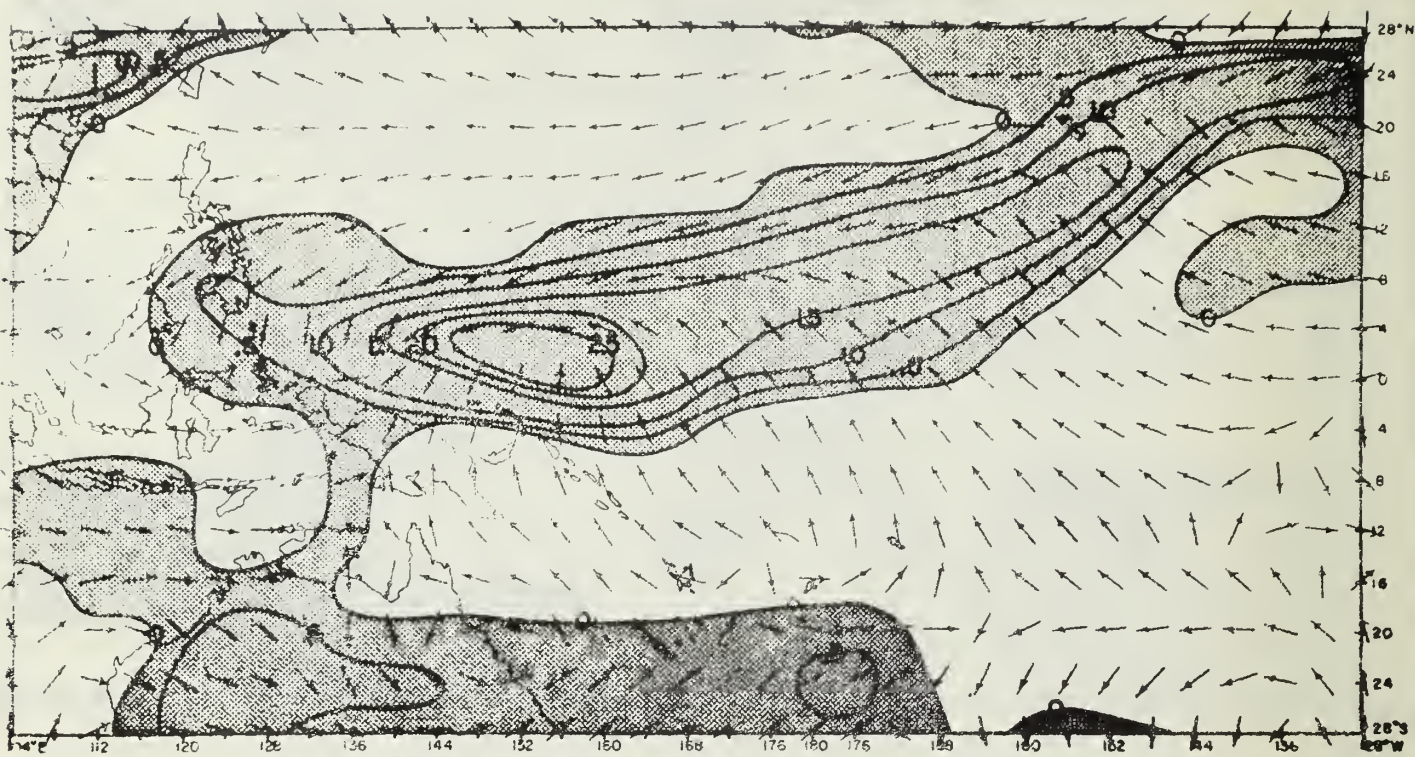


Figure 10. (c)

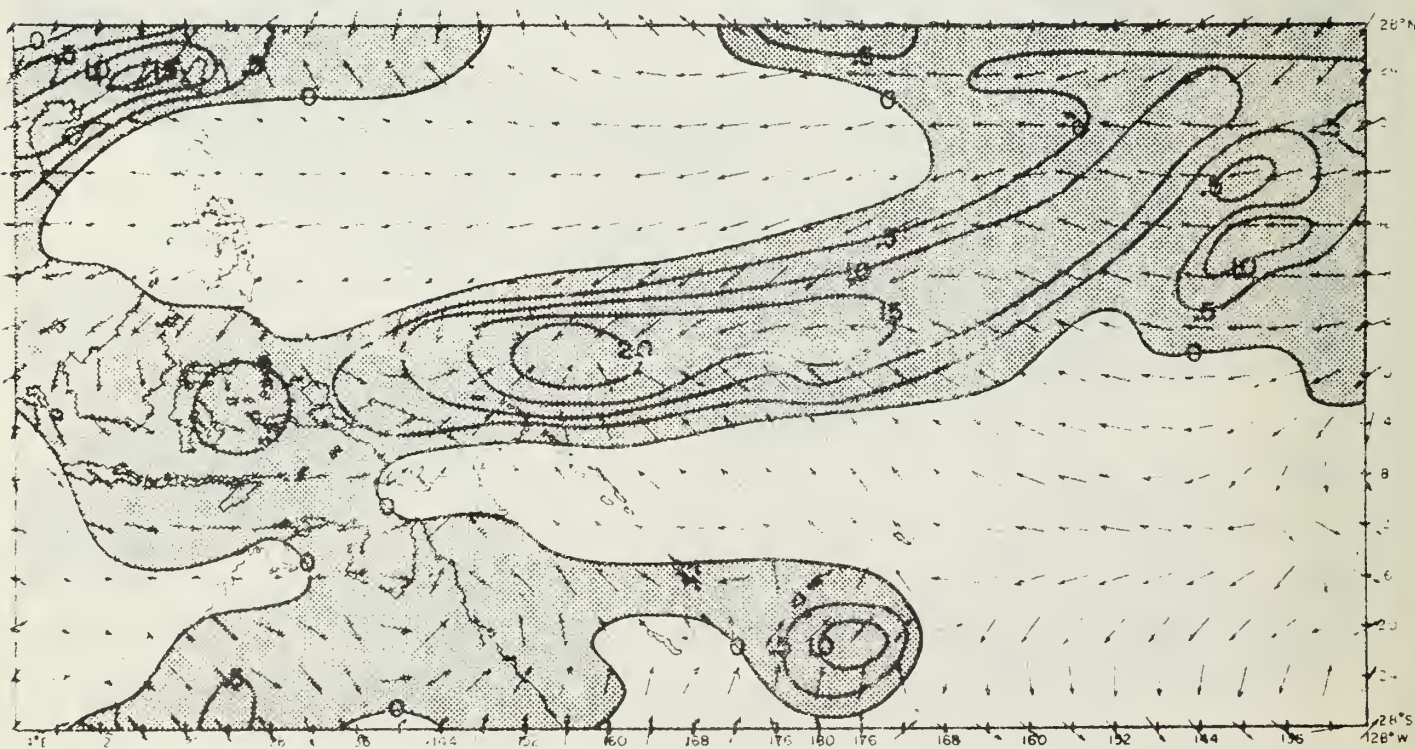


Figure 10. (d)

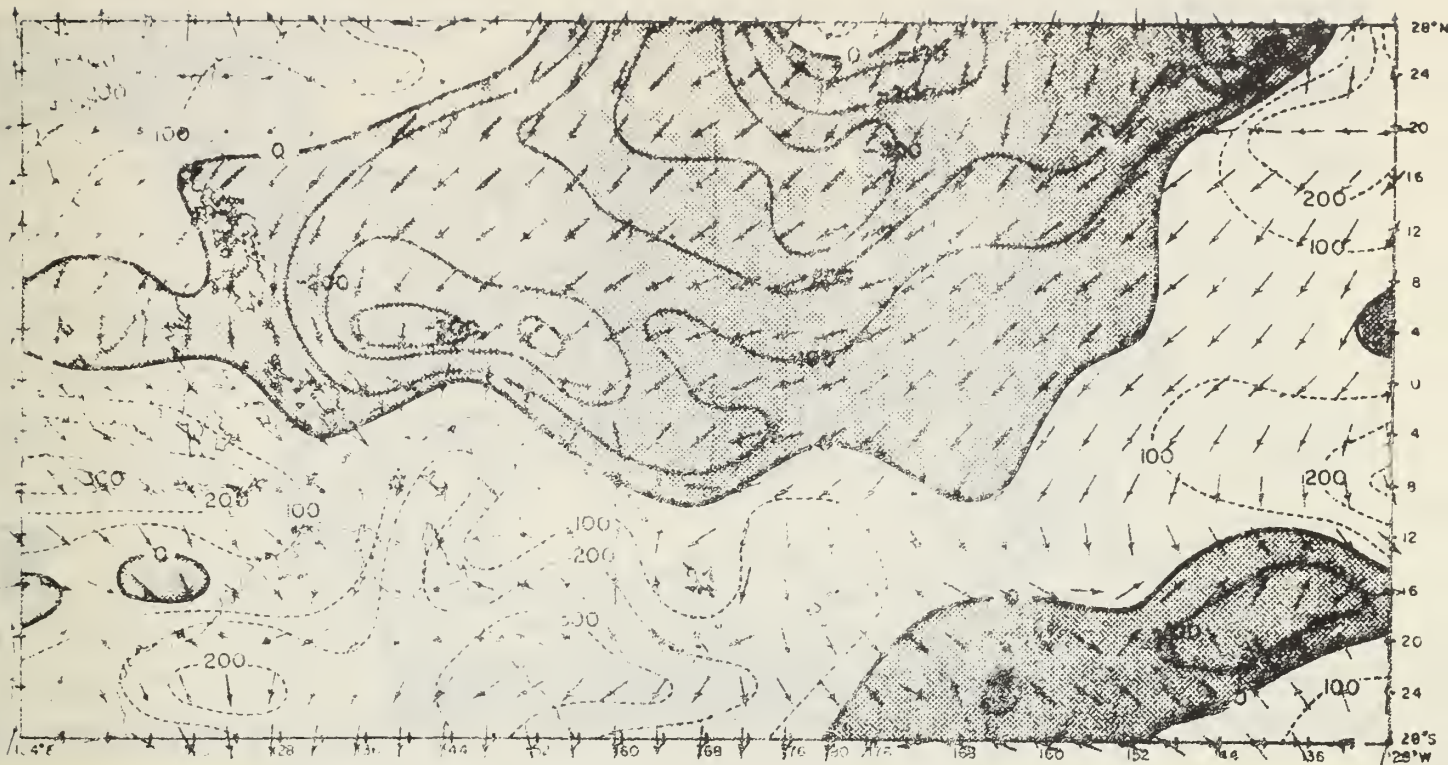


Figure 11. (a, b, c, & d) 6-, 12-, 18-, and 24-hour forecast of the distribution of 900-millibar vertical motions, units 10^{-5} millibar/sec, the shaded region indicates rising motions. The wind arrows are the directions of the forecast wind vectors at the 1000 mb surface.

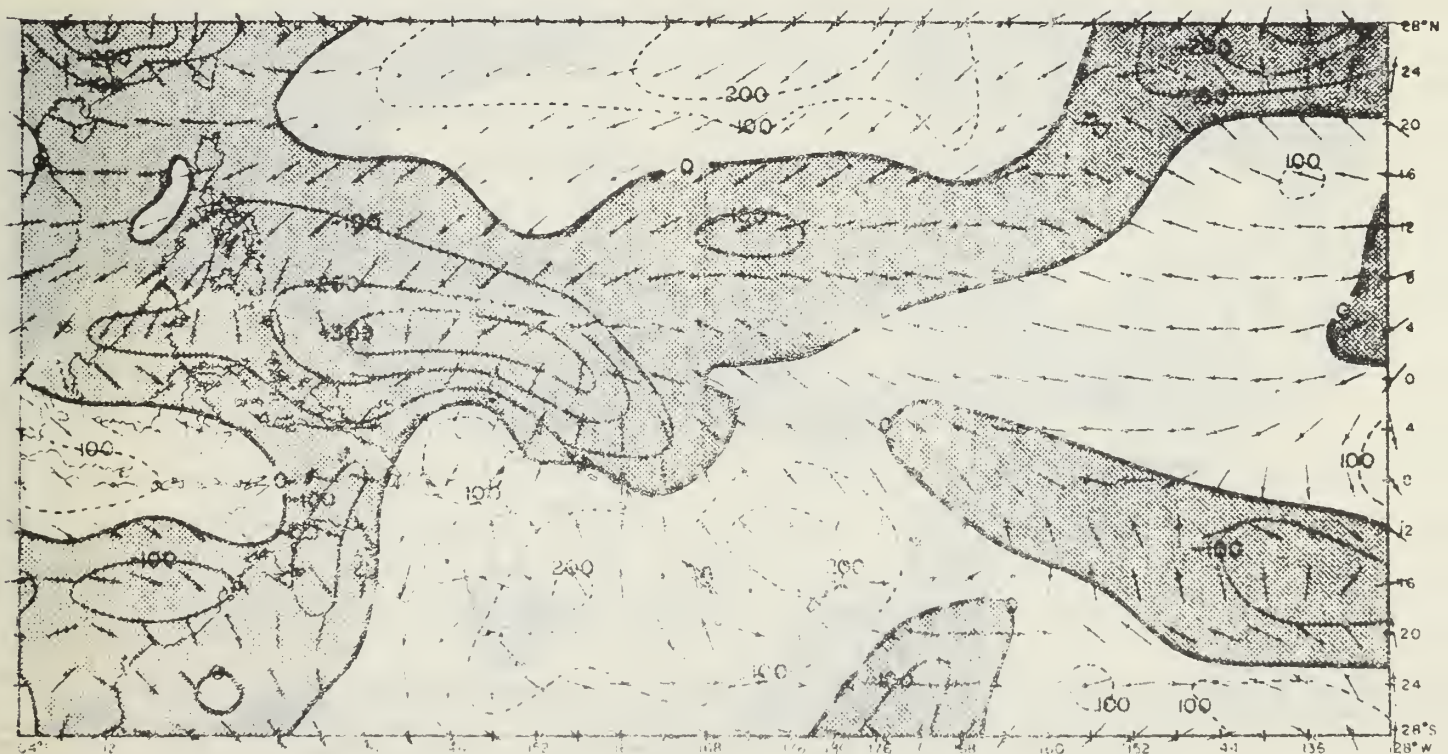


Figure 11. (b)

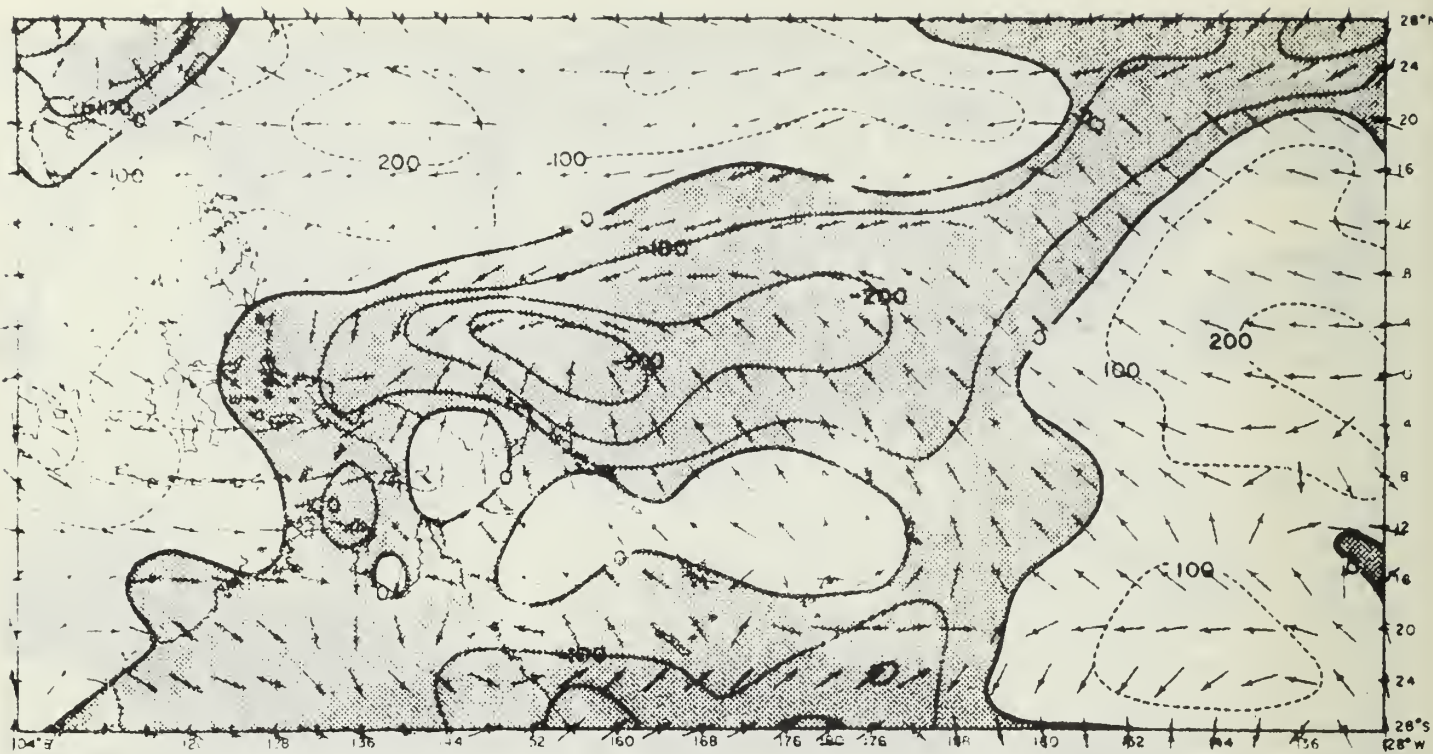


Figure 11. (c)

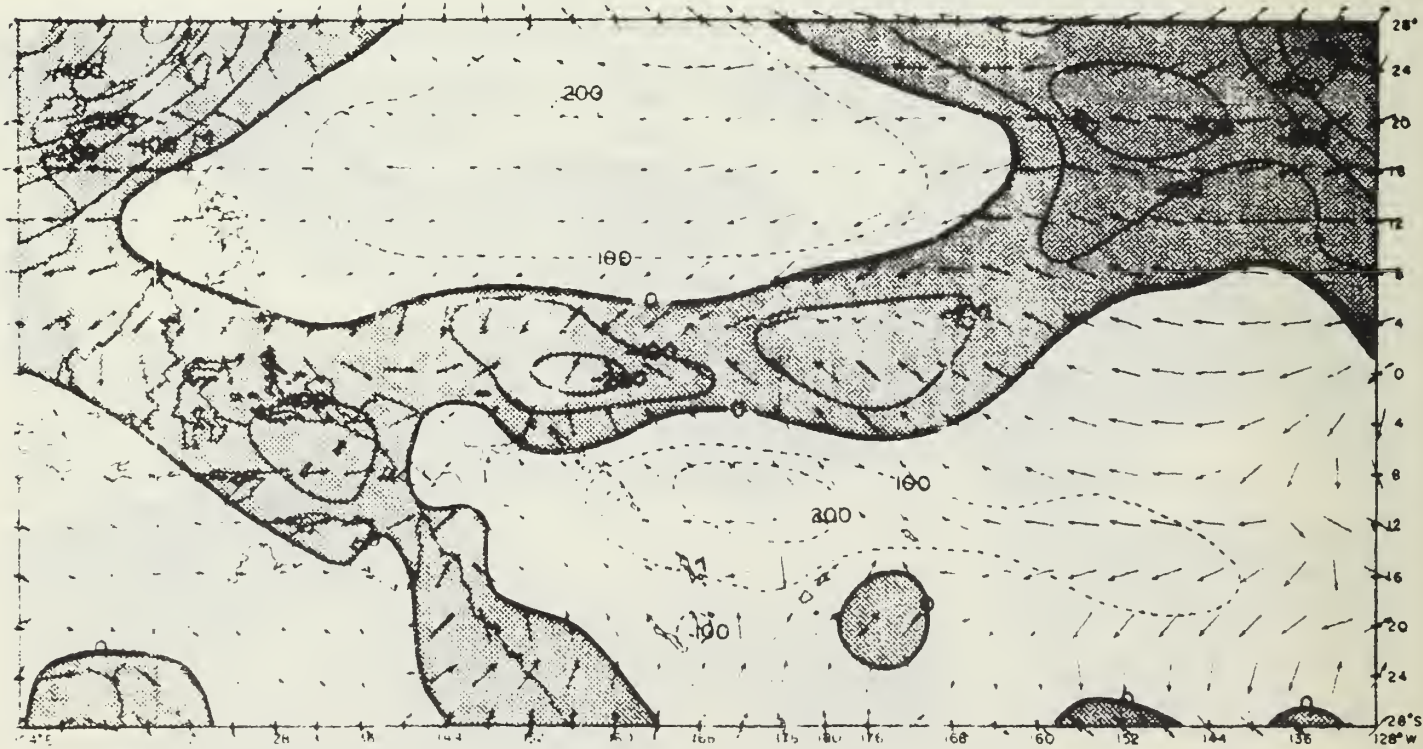


Figure 11. (d)

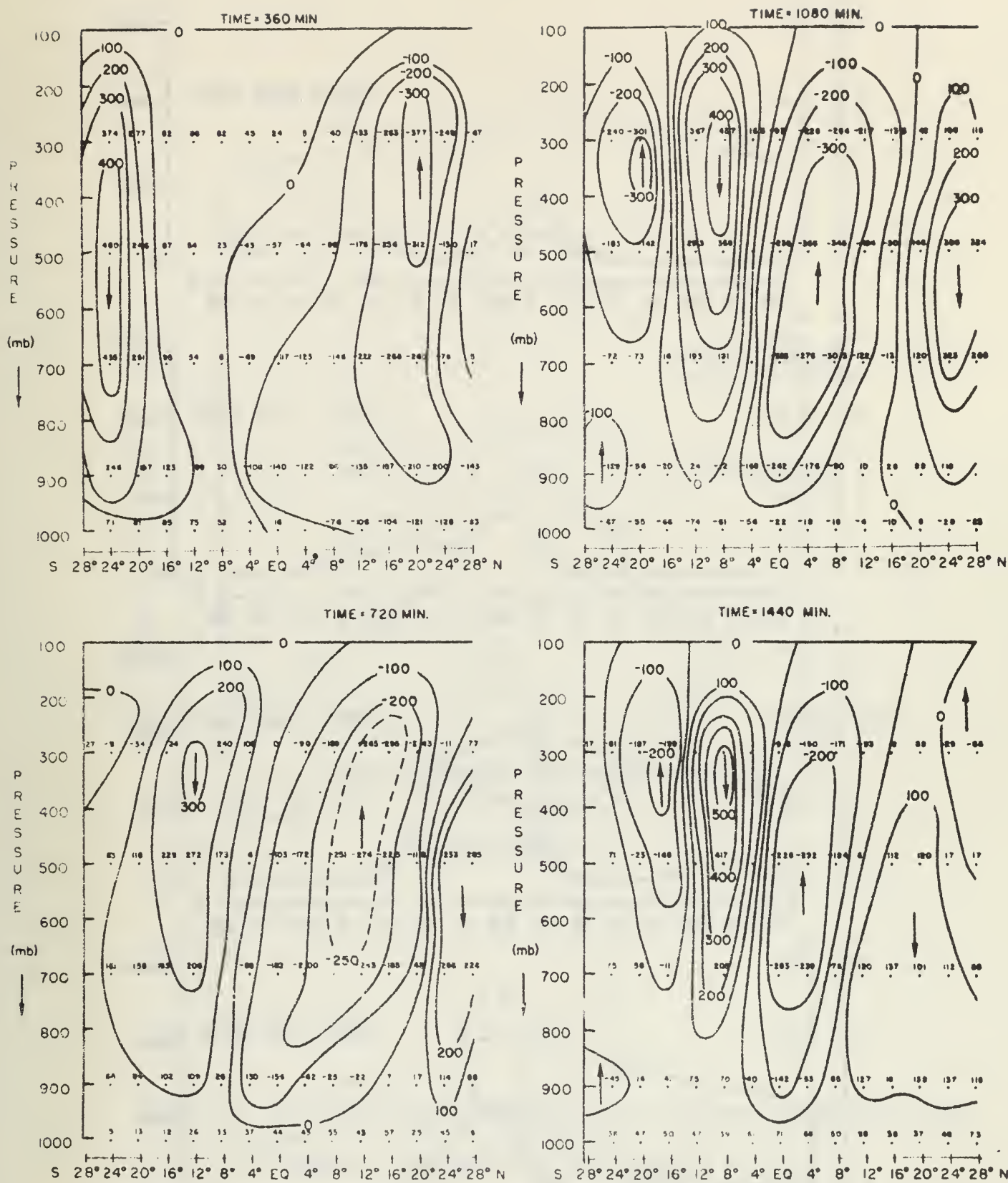


Fig. 12. Vertical cross-section of vertical motion (10^{-5} millibar/sec)

at 6, 12, 18 and 24 hours of forecast time. This cross section is taken in a south-north plane at 152°W longitude, and it intersects the ITCZ.

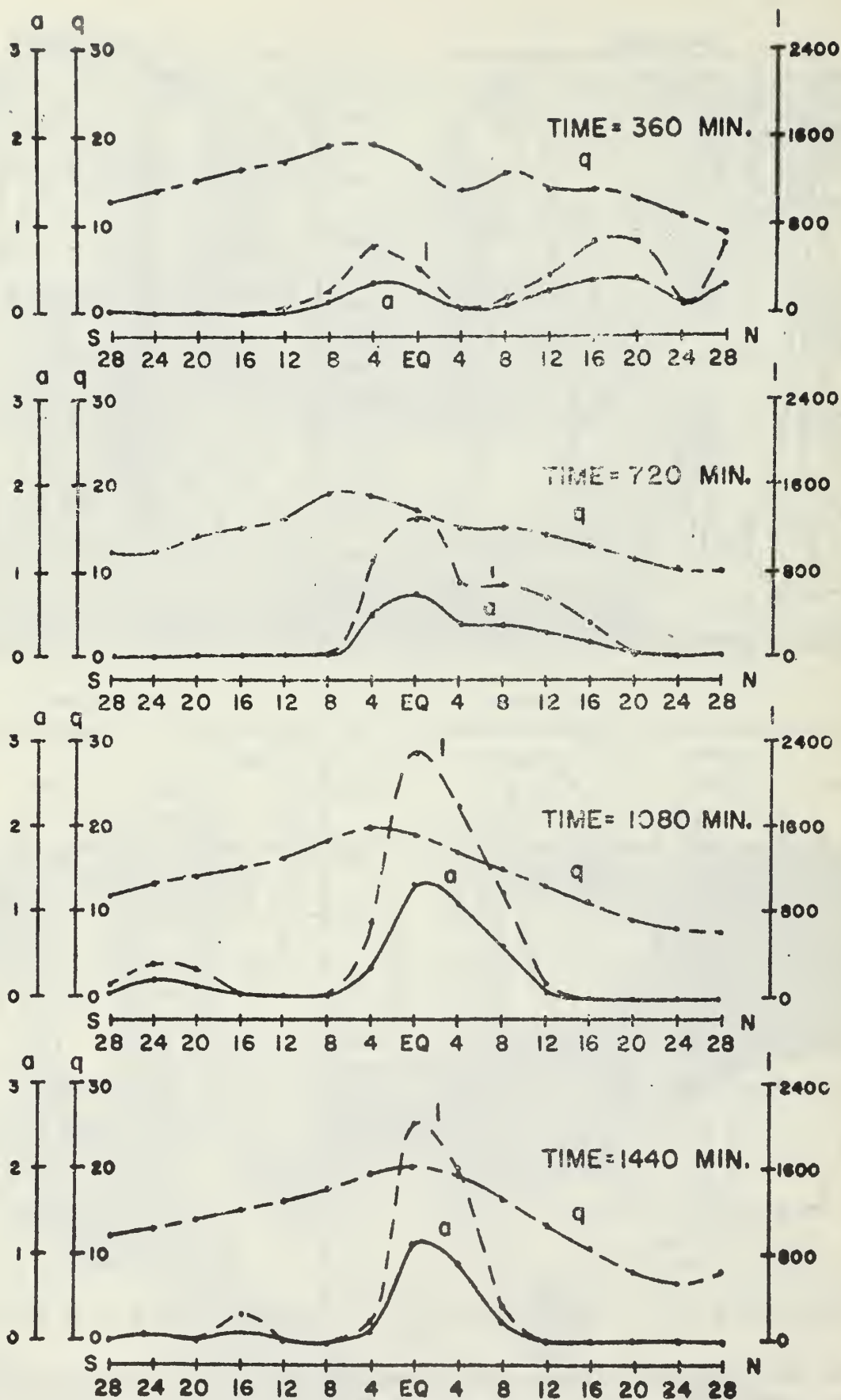


Figure 13. Time variation (along ordinate) of selected parameters at 152° W from south to north (along abscissa).

q specific humidity at 900 mb gm/kgm
a percent cloud cover
I net moisture convergence (10^{-8} mb meter⁻¹ sec)

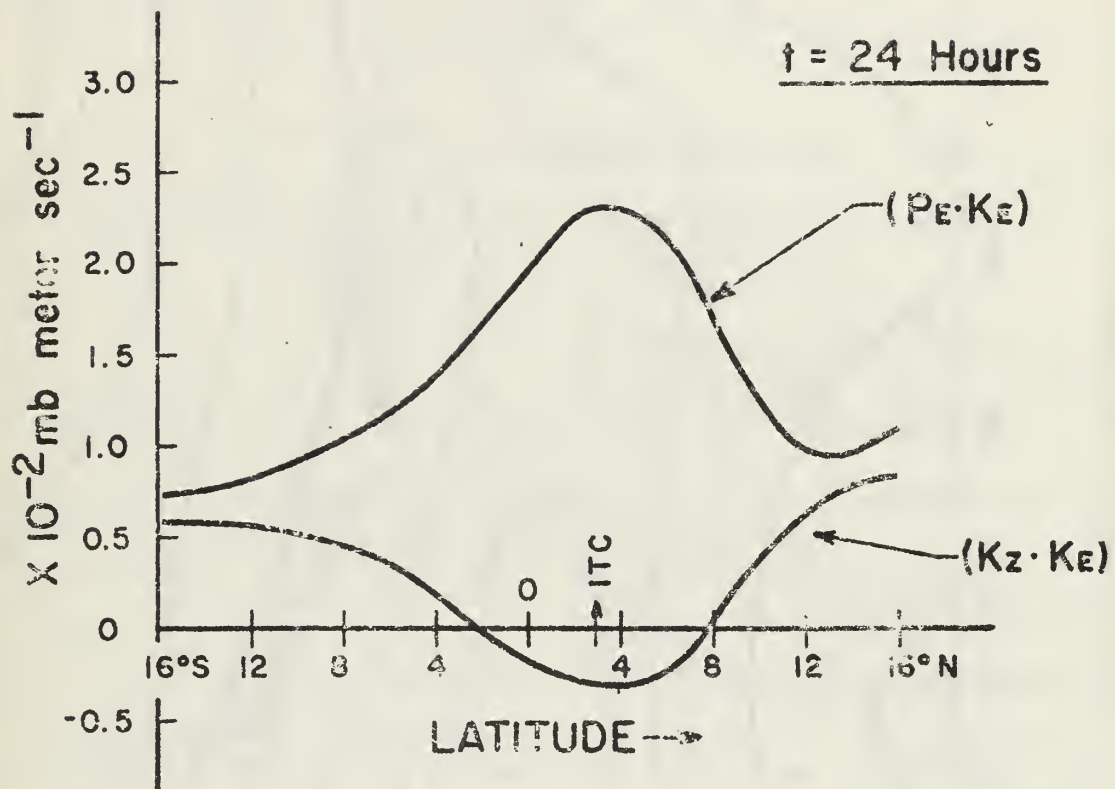


Figure 14. Selected energy conversions at $t = 24$ hours of forecast time, evaluated from equations (45) and (46) of text.

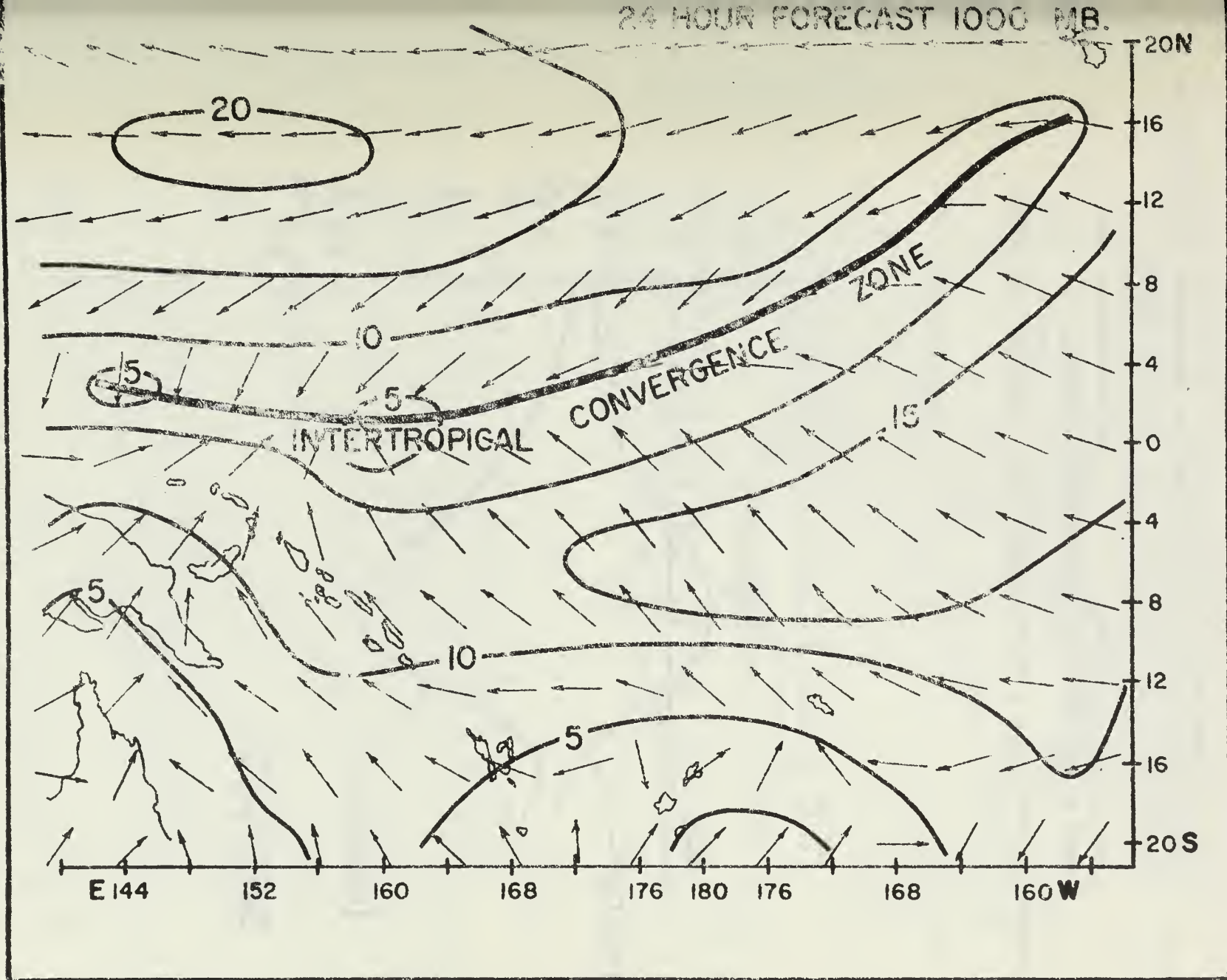


Figure 15. An enlarged view of the 1000 mb, 24-hour forecast of wind directions (arrows) and wind speeds (knots, solid lines) in the vicinity of the ITCZ (heavy dark line).

DOCUMENT CONTROL DATA - R & D

Security classification of title, body of abstract and indexing annotation must be entered when the overall report is classified

1. ORIGINATING ACTIVITY (Corporate author) Naval Postgraduate School Department of Meteorology and Oceanography Monterey, California 93940		2a. REPORT SECURITY CLASSIFICATION Unclassified	
		2b. GROUP	
3. REPORT TITLE AN EXPERIMENT IN NUMERICAL PREDICTION IN EQUATORIAL LATITUDES.			
4. DESCRIPTIVE NOTES (Type of report and, inclusive dates) Scientific Interim.			
5. AUTHOR(S) (First name, middle initial, last name) T. N. Krishnamurti			
6. REPORT DATE October 1968	7a. TOTAL NO. OF PAGES 75	7b. NO. OF REFS 43	
8a. CONTRACT OR GRANT NO. MIPR ES-7-967	9a. ORIGINATOR'S REPORT NUMBER(S) NPS-51KJ8081A Scientific Report No. 4		
b. PROJECT NO. 6698-02-01			
c. 62405394	9b. OTHER REPORT NO(S) (Any other numbers that may be assigned this report) AFCRL-68-0453		
d. 681000			
10. DISTRIBUTION STATEMENT Distribution of this document is unlimited. It may be released to the clearing house, Dept. of Commerce for sale to the general public.			
11. SUPPLEMENTARY NOTES TECH, OTHER		12. SPONSORING MILITARY ACTIVITY Air Force Cambridge Research Laboratories (CRH) L. G. Hanscom Field, Bedford, Mass. 01730	

13. ABSTRACT

In order to obtain the dynamical structure of the tropical atmosphere in equatorial latitudes a short range prediction experiment is proposed. The initial field contains the intertropical convergence zone and associated disturbances over western Pacific Ocean during March 1965. A complete initial state is constructed using a consistent balance system of equations. The procedure involves construction of pressure, temperature and vertical motion distributions starting from an observed rotational part of the wind field. It is shown that this procedure, whose validity assumes a small Rossby number, does not yield a realistic structure of the vertical motion. A short range prediction with a multi-level prediction model yields some interesting solutions in the vicinity of the intertropical convergence zone. During the first 18 hours of prediction an adjustment of the motion and the mass field ensues with gravity inertia oscillations. A detailed discussion of some dynamical aspects at 24 hours is presented. An important feature of the model is a parameterization of cumulus convection as a function of large-scale moisture convergence. The role of cumulus scale heating in the vicinity of the intertropical convergence zone is explored by carrying out experiments with and without diabatic heating.

14

KEY WORDS

LINK A

LINK B

LINK C

ROLE

WT

ROLE

WT

ROLE

WT

Tropical Weather prediction
Tropical Dynamics